J. Fluid Mech. (2003), *vol.* 478, *pp.* 165–196.
DOI: 10.1017/S002211200200335X Printed in the United Kingdom

The influence of non-equilibrium surfactant dynamics on the flow of a semi-infinite bubble in a rigid cylindrical capillary tube

By SAMIR N. GHADIALI AND DONALD P. GAVER III†

Department of Biomedical Engineering, Tulane University, New Orleans, LA 70118, USA

(Received 5 February 2002 and in revised form 24 September 2002)

We have utilized a computational model of semi-infinite air bubble progression in a surfactant-doped, fluid-filled rigid capillary to investigate the continual interfacial expansion dynamics that occur during the opening of collapsed pulmonary airways. This model simulates mixed-kinetic conditions with nonlinear surfactant equations of state similar to those of pulmonary surfactant. Several dimensionless parameters govern the system responses: the capillary number (Ca) that relates viscous to surface tension forces; the elasticity number (El), a measure of the ability of surfactant to modify the surface tension; the bulk Péclet number (Pe), relating bulk convection rates to diffusion rates; the adsorption and desorption Stanton numbers (St_a and St_d) that relate the adsorption/desorption rates to surface convective rates; and finally the adsorption depth (λ), a dimensionless bulk surfactant concentration parameter. We investigated this model by performing detailed parameter variation studies at fixed and variable equilibrium concentrations. We find that the surfactant properties can strongly influence the interfacial pressure drop through modification of the surface tension and the creation of Marangoni stresses that influence the viscous stresses along the interface. In addition, these studies demonstrate that, depending upon the range of parameters, either film thickening or film thinning responses are possible. In particular, we find that when $Pe \gg 1$ (as with pulmonary surfactant) or when sorption rates are low, concentration profiles can substantially differ from near-equilibrium approximations and can result in film thinning. These responses may influence stresses on epithelial cells that line pulmonary airways and the stability of these airways, and may be important to the delivery of exogenous surfactant to deep regions of the lung.

1. Introduction

The lung contains a bifurcating network of large and small airways which conduct air to and from the alveoli – the primary site of gas exchange with the blood. Closure of the small airways can occur when the lung reaches very low volumes (Levitzky 1991). Healthy adults are able to reopen these airways on the next inspiratory effort. However, patients suffering from emphysema and cystic fibrosis, and infants with respiratory distress syndrome cannot generate the pressures required to reopen their airways. These conditions often result in atelectasis and/or local hypoventilation. Pulmonary surfactant insufficiency, deficient tethering forces, and an increase in fluid

† Author to whom correspondence should be addressed: donald.gaver@tulane.edu

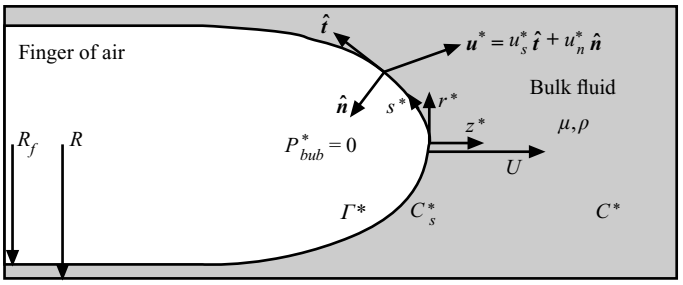

FIGURE 1. Schematic representation of the theoretical model in an axisymmetric coordinate system.

viscosity have been suggested as possible mechanisms by which airways remain closed (Enhörning & Holm 1993; Gaver, Samsel & Solway 1990; Kamm & Schroter 1989; Macklem, Proctor & Hogg 1970; Otis *et al.* 1993; Perun & Gaver 1995).

Airway closure occurs when a liquid occlusion spans the airway and blocks airflow. This occlusion can be extensive (as occurs prior to an infant's first breath or in atelectasis), or consist of a short meniscus (i.e. a mucous plug). The research described in this paper relates to reopening an extended region of closure, wherein a semi-infinite air bubble penetrates and displaces the liquid occlusion (see figure 1). A classic problem in the hydrodynamic literature related to pulmonary airway reopening involves semi-infinite bubble progression in a rigid capillary tube. This system was originally studied by Bretherton (1961), Fairbrother & Stubbs (1935) and Taylor (1961). These asymptotic studies formulated a relationship between the dimensionless interfacial pressure drop, $P^*/(\gamma^*/R)$ and the capillary number, $Ca = \mu U/\gamma^*$ in the limit of small Ca. P^* is the dimensional pressure drop across the air–liquid interface near the bubble tip, γ^* is the surface tension, R is the radius of the tube, μ is the fluid viscosity, and U is the bubble speed. Ca is a dimensionless velocity that represents the relationship of viscous to surface tension stresses. In addition, several numerical studies (Lu & Chang 1989; Martinez & Udell 1989; Reinelt & Saffman 1985; Shen & Udell 1985; Westborg & Hassager 1989) have extended these results to large Ca (i.e. $O(1)$) and have elucidated the flow field surrounding the bubble. These simulations show that at low Ca a diverging stagnation ring exists that directs fluid towards both the tip and thin film (see figure 6*b*). As Ca increases, this stagnation ring merges with the tip, and directs fluid unidirectionally towards the thin film (see figure 6*a*). This behaviour has important implications for surfactant deposition. However, these studies assumed a constant γ^* and therefore neglected the influence of surfactant. Surfactant modifies the flow field by altering the local surface tension and mechanical stress balance at the air–liquid interface. In rigid tubes, these interactions modify the interfacial shape, flow patterns and pressure drop and therefore affect interfacial dynamics.

In coupling surfactant physicochemistry and fluid mechanics it is important to understand the mechanisms of surfactant action and transport. Surfactant can reside in two phases: a bulk phase, C^*, and a surface phase, Γ^*. The surface phase directly modifies the interfacial surface tension by the surfactant equation of state, $\gamma^* = f(\Gamma^*)$. In general, the equation of state is a nonlinear function where increasing Γ^* reduces γ^*; however regions exist where $\mathrm{d}\gamma^*/\mathrm{d}\Gamma^*$ is nearly zero (Tchoreloff *et al.* 1991). In a static system, an equilibrium relationship between C^* and Γ^* exists, with an associated equilibrium surface tension γ_{eq}. The interface becomes saturated with surfactant as

C^* increases, resulting in a maximum equilibrium surface concentration Γ_{sat}, which determines the minimum equilibrium surface tension in a static system, γ_{sat}. In a dynamic system, Γ^* (and thus γ^*) can vary as a function of interfacial position. In addition, Γ^* can exceed Γ_{sat} under dynamic conditions due to surface compression (as occurs in the alveoli *in vivo* or experimentally in a Langmuir trough), which can reduce γ^* significantly (Krueger & Gaver 2000; Tchoreloff *et al.* 1991).

The transport of surfactant to the interface can be described by a two-step serial process. First, bulk surfactants are convected and diffused to (or away from) a region near the interface, the sub-surface. The mass flux of surfactant (j_n^*) due to bulk transport processes is a function of the bulk concentration field, $C^*(r^*, z^*)$. Second, surfactant molecules are adsorbed onto (or desorbed from) the interface. The mass flux of surfactant due to adsorption/desorption processes is a function of both the sub-surface concentration, C_s^*, and the interfacial concentration, Γ^*. The overall transport or flux of surfactant to the interface is limited by the slower of these two processes. Specifically, if the bulk transport of surfactant is much faster than the adsorptive transport the system is classified as a *bulk-equilibrium* case. Under these conditions, the bulk concentration will be uniform and the bulk transport equation does not have to be explicitly solved. On the other hand, if the adsorptive transport is much faster than the bulk transport the system is classified as a *diffusion-limited* case. Under these conditions, Γ^* is always in equilibrium with C_s^* and the surface transport equation does not have to be explicitly solved. Therefore, the bulk and surface transport equations are decoupled and do not have to be solved simultaneously under bulk-equilibrium or diffusion-limited conditions. However, when the bulk and adsorptive transport rates are comparable the bulk and surface transport equations are coupled and must be solved simultaneously. Under these conditions the system is classified as a *mixed-kinetics* case. These transport interactions determine the distribution of surfactant in the bulk and along the interface. This distribution establishes a stress balance along the interface via the equation of state and thus has an impact on airway reopening pressures and stresses.

Several investigators (Ginley & Radke 1988; Ratulowski & Chang 1990; Stebe & Barthès-Biesel 1995) have studied the interaction between surfactant physicochemistry and fluid mechanics in a semi-infinite bubble progression model. Ratulowski & Chang (1990) found that the presence of trace quantities of surfactants could increase the dimensionless opening pressure, $P^*/(\gamma^*/R)$, under diffusion-limited conditions. However, this model is not capable of simulating large deviations from equilibrium and/or elevated surfactant concentrations. Stebe & Barthès-Biesel (1995) demonstrated that an increase in $P^*/(\gamma^*/R)$ could also occur at elevated surfactant concentrations if the adsorption processes were slow. Note that these studies are only valid for low Ca. Since all transport parameters are scaled with Ca, these studies can not simulate $O(1)$ deviations from equilibrium. In contrast the current numerical model is able to simulate large values of Ca and surfactant transport parameters.

The most common technique to compute non-equilibrium surfactant interactions in a free-surface system is a combined boundary element method (BEM) to solve Stokes flow equations and finite difference method to solve the surface transport equations. For an insoluble surfactant, the bulk concentration is not important since surfactant molecules reside only on the interface. Stone & Leal (1990) investigated the deformation and breakup of liquid drops, while Milliken, Stone & Leal (1993) and Eggleton, Pawar & Stebe (1999) studied the stretching of a viscous drop under uniaxial extensional flow conditions. Recently, Johnson & Borhan (1999) used the boundary

integral technique to study the effects of surfactant on the motion and deformation of finite liquid drops in Poiseuille flow through circular tubes. Gaver *et al.* (1996) used the boundary element method to investigate bubble progression in a flexible airway while Yap & Gaver (1998) used this technique to investigate the importance of surfactant physicochemistry for an idealized surfactant under bulk-equilibrium conditions. They predicted that surfactant uptake could significantly influence the mechanics of airway reopening.

The hybrid BEM–finite difference techniques described above cannot simulate the bulk-phase convection–diffusion transport dynamics of surfactant. However, experiments have demonstrated that the bulk transport of pulmonary surfactants can significantly influence the physicochemical hydrodynamic behaviour of the system (Ghadiali & Gaver 2000). In a recent paper (Ghadiali, Halpern & Gaver 2001), we have developed a computational model that is capable of simulating bulk surfactant transport dynamics under non-equilibrium conditions. This model is capable of simulating bulk-equilibrium and diffusion-limited conditions as well as the coupled transport process that occur under mixed-kinetic conditions. In addition, this computational model is able to simulate the nonlinear surfactant equations of state expressed by pulmonary surfactants (Lipp *et al.* 1996; Taneva & Keough 1994).

The goal of the present study is to use this computational model to investigate how various surfactant physicochemical properties, such as adsorption rate, can influence the fluid dynamics of semi-infinite bubble progression in a rigid tube. First, a set of dimensionless parameters that represent the relative magnitude of these physicochemical properties is obtained by scaling the appropriate hydrodynamic, surfactant transport and interfacial mechanics equations. An extensive parametric study is conducted in which each parameter is varied independently to investigate the influence of a given physicochemical property. Specifically, we seek solutions for the interfacial geometry, concentration profiles and interfacial pressure drop as a function of the dimensionless parameters. In addition, we calculate the interfacial surface velocities and the bulk flow patterns that result from bubble motion. Analysis of these simulations leads to a more complete understanding of the basic physicochemical hydrodynamic interactions in this system. We also obtain an understanding of how various bulk transport properties not considered heretofore can affect the mechanics of pulmonary airway reopening. Knowledge of how these properties interact with the fluid mechanical environment may lead to the development of more effective pulmonary surfactant replacement therapies.

2. Model formulation

The theoretical model of semi-infinite bubble progression in a rigid axisymmetric capillary tube with a radius R is demonstrated in figure 1. The displaced fluid, which can contain surfactant, has a viscosity μ and density ρ. We consider the steady-state movement of this bubble with a forward velocity U. The air–liquid interface is defined at each point by a unit normal, $\hat{\boldsymbol{n}} = (n_z, n_r)$, and a unit tangent, $\hat{\boldsymbol{t}} = (t_z, t_r)$, vector. The gas-phase viscosity is assumed to be negligible, and the finger width in the thin film region is defined as R_f, and is found as part of the solution. The reference pressure is the bubble pressure, $P^*_{bub} = 0$. Surfactant molecules can exist either in the bulk solution with concentration C^* or adsorbed onto the interface with concentration Γ^*. The model is based on the basic governing equations for fluid mechanics, molecular transport and interfacial dynamics.

2.1. *Surfactant transport equations*

The governing equation for convection and diffusion of surfactant in the bulk solution is

$$\frac{\partial C^*}{\partial t^*} + (\boldsymbol{u}^* \cdot \nabla^*) C^* = D_{mol} \nabla^{*^2} C^*. \tag{2.1}$$

Here, an asterisk is used to denote dimensional variables, $\boldsymbol{u}^*$ is the velocity vector and D_{mol} is the bulk diffusion coefficient. The concentration of surfactant on the interface, Γ^*, is governed by a conservation equation derived by Stone (1990):

$$\frac{\partial \Gamma^*}{\partial t^*} + \nabla_s^* \cdot (\Gamma^* \boldsymbol{u}_s^*) + \Gamma^* (\nabla_s^* \cdot \hat{\boldsymbol{n}})(\boldsymbol{u}^* \cdot \hat{\boldsymbol{n}}) = D_{int} \nabla_s^{*^2} \Gamma^* + j_{\boldsymbol{n}}^*. \tag{2.2}$$

Here ∇_s^* is a surface gradient operator, $\boldsymbol{u}_s^*$ is the surface velocity, D_{int} is the surface diffusion coefficient, and j_n^* is the mass flux to the interface from the bulk.

As stated above, the mass flux to the interface occurs in a two-step serial process. The first step involves diffusion from the bulk. In this case j_n^* is given by Fick's Law,

$$j_{\boldsymbol{n}}^* = -D_{mol} (\hat{\boldsymbol{n}} \cdot \nabla^*) C^*. \tag{2.3}$$

The second step involves an adsorption/desorption process from the subsurface to the interface. In this study we utilize Langmuir adsorption kinetics to determine the form of j_n^*. Specifically, the adsorption rate term is proportional to the sub-surface concentration as well as the number of free sites, while the desorption rate is proportional to the number of filled sites,

$$j_{\boldsymbol{n}}^* = k_L^a C_s^* [\Gamma_\infty - \Gamma^*] - k_L^d \Gamma^*. \tag{2.4}$$

The surface concentration when all sites are filled is the maximum monolayer packing concentration, Γ_∞, which equals Γ_{sat}. Continuity at the interface dictates a balance of diffusive and sorptive fluxes,

$$k_L^a C_s^* [\Gamma_\infty - \Gamma^*] - k_L^d \Gamma^* = -D_{mol} (\hat{\boldsymbol{n}} \cdot \nabla^*) C^*. \tag{2.5}$$

This flux balance equation will be used as a boundary condition when solving the bulk transport equation (2.1), while j_n^* in the surface transport equation (2.2) will be associated with the adsorptive/desorptive flux term, equation (2.4).

2.2. *Langmuir equation of state*

To determine the Langmuir equation of state that relates surface tension to surface concentration, $\gamma^*(\Gamma^*)$ we utilize an adsorption equilibrium relationship, i.e. equation (2.4) with $j_n^* = 0$,

$$\frac{\Gamma^*}{\Gamma_\infty} = \frac{K_L C_s^*}{1 + K_L C_s^*}, \tag{2.6}$$

where $K_L = k_L^a / k_L^d$. In order to determine $\gamma^*(\Gamma^*)$ we also utilize the Gibb's thermodynamic relationship (Myers 1991),

$$\mathrm{d}\gamma^* = -\mathbb{R} T \Gamma^* \mathrm{d}(\ln C_s^*), \tag{2.7}$$

which relates surface tension to the sub-surface and interfacial concentrations. Here, $\mathbb{R}$ is the universal gas constant and T is the temperature. Equations (2.6) and (2.7) can be used to obtain the Langmuir equation of state,

$$\gamma^*(\Gamma^*) = \gamma_{eq} + \mathbb{R} T \Gamma_\infty \ln\left(\frac{\Gamma_\infty - \Gamma^*}{\Gamma_\infty - \Gamma_{eq}}\right). \tag{2.8}$$

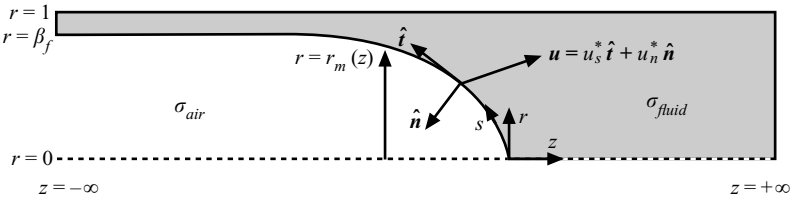

FIGURE 2. Schematic of the fluid boundary and the location of the imposed boundary conditions.

Here Γ_{eq} is the surface concentration that is in equilibrium with the far-field bulk concentration, C_o, and γ_{eq} is the associated equilibrium surface tension. Note that equation (2.8) contains a logarithmic singularity as $\Gamma^* \to \Gamma_\infty$ such that $\gamma^* \to -\infty$. As demonstrated in other studies (Eggleton *et al.* 1999) as well as the present one, the highly nonlinear behaviour of equation (2.8) near the singularity generates a large mechanical response (i.e. large Marangoni stress) that ensures that $\Gamma^* < \Gamma_\infty$. Therefore, this singularity does not require special computational treatment.

2.3. *Dimensionless governing equations and boundary conditions*

We use the following scaling arguments to obtain dimensionless governing equations.

$$\left.\begin{gathered} s^* = Rs, \quad r^* = Rr, \quad z^* = Rz, \quad \boldsymbol{u}^* = U\boldsymbol{u}, \\ C^* = C_o C, \quad \gamma^* = \gamma_{eq}\gamma, \quad \Gamma^* = \Gamma_\infty \Gamma, \quad P^* = \frac{\gamma_{eq}}{R}\Pi. \end{gathered}\right\} \tag{2.9}$$

Here P^* is the pressure, s is the arclength coordinate and C_o is the far-downstream bulk concentration. When inertial forces are negligible ($Re = \rho UR/\mu \ll 1$), the scaled form of the Navier–Stokes equations reduces to the steady-state Stokes equations,

$$\nabla \Pi = Ca \nabla^2 \boldsymbol{u}, \quad \nabla \cdot \boldsymbol{u} = 0, \tag{2.10}$$

where $Ca = \mu U/\gamma_{eq}$ is the capillary number that relates viscous to surface tension forces.

Steady-state boundary conditions on the domain shown in figure 2 are

$$\frac{\partial u_z}{\partial r} = 0, \quad u_r = 0 \quad \text{at} \quad z > 0, \quad r = 0, \tag{2.11}$$

$$\boldsymbol{u} \cdot \hat{\boldsymbol{n}} = u_z n_z + u_r n_r = 0 \quad \text{at} \quad r = r_m(z), \tag{2.12}$$

$$\boldsymbol{\sigma}_{fluid} \cdot \hat{\boldsymbol{n}} = \gamma \kappa \hat{\boldsymbol{n}} + \frac{\mathrm{d}\gamma}{\mathrm{d}s}\hat{\boldsymbol{t}} \quad \text{at} \quad r = r_m(z), \tag{2.13}$$

$$u_z = -1, \quad u_r = 0 \quad \text{as} \quad z \to -\infty, \tag{2.14}$$

$$u_r = 0, \quad u_z = -1 \quad \text{at} \quad r = 1, \tag{2.15}$$

$$u_z = -\left[2\beta_f^2(r^2 - 1) + 1\right], \quad u_r = 0 \quad \text{as} \quad z \to +\infty. \tag{2.16}$$

Here $\beta_f = R_f/R$ is the dimensionless width of the air bubble in the thin film. Equation (2.11) specifies symmetry at the centreline. The kinematic boundary conditions ((2.12), (2.14), (2.15) and (2.16)) are stated in terms of the bubble-fixed reference frame at steady state. Equation (2.12) specifies no penetration at the interface while (2.15) specifies no slip at the tube wall. Equation (2.14) imposes a plug-flow boundary condition in the static thin film while (2.16) imposes Poiseuille flow far downstream. Note that (2.16) satisfies a global conservation of mass relationship. Finally, (2.13)

represents the interfacial stress balance where $\boldsymbol{\sigma}_{fluid} = -\Pi \boldsymbol{I} + Ca(\nabla \boldsymbol{u} + \nabla^T \boldsymbol{u})$ represents the fluid stress tensor and $\boldsymbol{\sigma}_{air} = 0$.

Since the interface is a free surface, a surface geometry must be determined that simultaneously satisfies boundary conditions for velocity (2.13) and stress (2.14). To do so, the stress balance (2.13) is imposed while the interface shape is iterated until (2.12) is satisfied.

Under steady-state conditions, the scaled form of (2.1) yields

$$(\boldsymbol{u} \cdot \nabla) C = Pe^{-1} \nabla^2 C. \tag{2.17}$$

Here $Pe = UR/D_{mol}$ is the bulk Péclet number which relates convection rates to diffusion rates. The following boundary conditions complete the bulk transport formulation:

$$\frac{\partial C}{\partial r} = 0 \quad \text{at} \quad r = 0, \tag{2.18}$$

$$(\hat{\boldsymbol{n}} \cdot \nabla) C = -PeSt_a C_s (1 - \Gamma) + PeSt_a \lambda \Gamma \quad \text{at} \quad r = r_m(z), \tag{2.19}$$

$$\frac{\partial C}{\partial z} = 0 \quad \text{as} \quad z \to -\infty, \tag{2.20}$$

$$\frac{\partial C}{\partial r} = 0 \quad \text{at} \quad r = 1, \tag{2.21}$$

$$C = 1 \quad \text{as} \quad z \to +\infty. \tag{2.22}$$

Here $\lambda = \Gamma_\infty / C_o R$ is the dimensionless adsorption depth and the adsorption parameters (St_a and St_d) are defined below. The adsorption depth is a length scale related to the fluid thickness that contains sufficient surfactant molecules to obtain an interfacial concentration of Γ_∞. The boundary conditions specify symmetry at the centreline (2.18), no axial variation in the static thin film (2.20), no surfactant flux into the tube wall (2.21), and a constant far-downstream bulk concentration (2.22). The interfacial boundary condition (2.19) specifies continuity between bulk diffusive and adsorptive/desorptive fluxes at the interface. Note that (2.19) is the dimensionless form of (2.5) using Langmuir kinetics for the adsorptive flux term, $f(C_s^*, \Gamma^*)$.

Under steady-state conditions $\boldsymbol{u} \cdot \hat{\boldsymbol{n}} = 0$, and the scaled form of (2.2) yields

$$\nabla_s \cdot (\Gamma \boldsymbol{u}_s) = Pe_s^{-1} \nabla_s^2 \Gamma + \frac{St_a}{\lambda} C_s (1 - \Gamma) - St_d \Gamma, \tag{2.23}$$

where we have used (2.4) for j_n^*. Here $Pe_s = UR/D_{int}$ is the surface Péclet number which relates surface convection rates to surface diffusion rates, $St_a = k_a \Gamma_\infty / U$ is the adsorption Stanton number that relates adsorption rates to surface convection rates, and $St_d = k_d R/U$ is the desorption Stanton number which relates desorption rates to surface convection rates. Note that $St_\lambda = St_a/\lambda$ is the effective adsorption parameter which relates adsorption rates to interfacial creation rates.

Finally, the following boundary conditions complete the transport of surfactant on the interface:

$$\frac{\partial \Gamma}{\partial s} = 0 \quad \text{at} \quad s = 0, \tag{2.24}$$

$$\frac{\partial \Gamma}{\partial s} = 0 \quad \text{as} \quad s^{\to \infty}. \tag{2.25}$$

These Neumann boundary conditions specify symmetry at the centreline (2.24) and no variation in the static thin film (2.25).

A scaling analysis of (2.8) yields the dimensionless Langmuir equation of state,

$$\gamma(\Gamma) = 1 + El \ln \frac{1-\Gamma}{1-\tilde{\Gamma}_{eq}} \tag{2.26}$$

Here $El = \mathbb{R}T\Gamma_\infty/\gamma_{eq}$ is the elasticity number, which is a measure of a surfactant's ability to modify the interfacial surface tension and $\tilde{\Gamma}_{eq} = \Gamma_{eq}/\Gamma_\infty$ is the dimensionless equilibrium surface tension where Γ_{eq} is in equilibrium with the far-field bulk concentration C_o. Note that (2.6) can be used to express $\tilde{\Gamma}_{eq}$ in terms of St_λ and St_d.

$$\tilde{\Gamma}_{eq} = \frac{St_\lambda}{St_\lambda + St_d}. \tag{2.27}$$

Although other investigators (Ratulowski & Chang 1990) have identified the measure of a surfactant's strength with the Marangoni number, Ma, we follow a more traditional definition (Stebe & Barthès-Biesel 1995) such that Ma is related to the ratio of Marangoni to viscous stresses, i.e. $Ma = El/Ca = \mathbb{R}T\Gamma_\infty/\mu U$.

2.4. *Solution methods*

The details of the solution technique are given in Ghadiali *et al.* (2001). Briefly, the boundary element method (BEM) is used to solve the fluid mechanics, the dual reciprocity boundary element method (DRBEM) is used to solve the transport of surfactant in the bulk, and a finite difference scheme (FDM) is used to solve the interfacial transport of surfactant. Note that under general conditions, the governing surfactant transport equations are coupled to the fluid mechanics via the stress balance at the interface (2.13) and the equation of state (2.26). Specifically, the velocity field, which is used to determine interfacial kinematics, depends on the stress balance at the interface. For a given $\gamma(s)$ the steady-state interfacial shape can be obtained by moving the interface according to kinematic relationships until the bubble shape does not change with time. Once this new shape is known, the fluid velocities, which will be different from the velocities associated with the previous shape, can be used to solve the surfactant transport equations for $\Gamma(s)$ and thus $\gamma(s)$. This new $\gamma(s)$, which alters the interfacial stress balance, will result in an altered flow field and therefore a new steady-state shape. Therefore, an iterative scheme in conjunction with a relaxation technique, described in detail by Ghadiali *et al.* (2001) is used to obtain a converged steady-state solution to the nonlinear hydrodynamic and surfactant transport governing equations. As a result, several system characteristics (including bubble tip pressure drop, Π_{tip}, tip curvature, κ_{tip}, tip surface tension, γ_{tip}, and finger width, β_f) can be determined for a given set of dimensionless parameters.

2.5. *Accuracy calculation*

The thin-film boundary conditions for the bulk and surface transport problems, equations (2.20) and (2.25), are defined at an infinite axial distance from the bubble tip. If the computational domain in the thin film is truncated prematurely, the application of these boundary conditions will result in an inaccurate solution. To assess solution accuracy we follow Ghadiali *et al.* (2001) and formulate an overall mass balance between regions far upstream and downstream of the tip. This mass balance can be expressed as

$$\tilde{\Gamma}_{film} = \frac{(1-\tilde{C}_{film})(1-\beta_f^2)}{2\lambda\beta_f}, \tag{2.28}$$

where $\tilde{C}_{film}$ and $\tilde{\Gamma}_{film}$ have constant values in the thin film. In addition, the thin-film

bulk and interfacial concentrations are in equilibrium and can be related to the dimensionless form of equation (2.6):

$$\tilde{\Gamma}_{film} = \frac{St_\lambda \tilde{C}_{film}}{St_\lambda \tilde{C}_{film} + St_d}. \tag{2.29}$$

As a result, $\tilde{C}_{film}$ can be determined from equations (2.28) and (2.29) for given dimensionless parameter values. The relative error between the thin-film concentration obtained from the numerical simulation and the analytical $\tilde{C}_{film}$ value is a measure of solution accuracy. This error was maintain at $< 1\%$ by either extending the solution domain or increasing the number of nodes in the BEM/DRBEM model.

2.6. *Bubble-tip pressure drop calculation*

Although the majority of the geometrical and mechanical properties (κ_{tip}, β_f, and γ_{tip}) are calculated as part of the iteration solution, the calculation of Π_{tip} requires some explanation. To calculate Π_{tip} we follow the technique presented in Martinez (1987). The normal stress component at the interface, $\hat{\boldsymbol{n}} \cdot (\boldsymbol{\sigma}_{fluid} \cdot \hat{\boldsymbol{n}})$, which according to the interfacial stress balance (2.13) is equal to $\gamma\kappa$, can be expressed in terms of the normal velocity at the interface, u_n:

$$\hat{\boldsymbol{n}} \cdot (\boldsymbol{\sigma}_{fluid} \cdot \hat{\boldsymbol{n}}) = -\Pi_{fluid} + 2Ca \frac{\partial u_n}{\partial n} = \gamma\kappa. \tag{2.30}$$

Conservation of mass in an axisymmetric normal–tangential (n–s) coordinate system indicates that

$$\frac{\partial u_n}{\partial n} = -\frac{1}{r}\frac{\partial (r u_s)}{\partial s}. \tag{2.31}$$

At the bubble tip, where $r = 0$, the limit of equation (2.31) can be used with equation (2.30) to determine the pressure drop across the interface ($\Pi_{tip} = \Pi_{air} - \Pi_{fluid}$),

$$\Pi_{tip} = -\Pi_{fluid} = \gamma_{tip}\kappa_{tip} + 4Ca \frac{\partial u_s}{\partial s}, \tag{2.32}$$

where Π_{fluid} is the fluid pressure at the tip and $\Pi_{air} = 0$ is the reference pressure. Therefore, Π_{tip} has a surface tension component ($\gamma_{tip}\kappa_{tip}$) and a viscous component ($4Ca\, \mathrm{d}u_s/\mathrm{d}s$).

2.7. *Fixed vs. variable equilibrium point calculations*

In § 3.4 we conduct a 'variable equilibrium point' study in which we allow the change in $\tilde{\Gamma}_{eq}$ to occur with changes in the dimensionless parameters. From (2.27) the equilibrium point, $\tilde{\Gamma}_{eq} = \Gamma_{eq}/\Gamma_\infty$, is a function of the adsorption depth parameter (λ), the adsorption Stanton number (St_a), and the desorption Stanton number (St_d). This change in $\tilde{\Gamma}_{eq}$ with the dimensionless parameters can be explained physically. For example, increasing the sorption rate St_a at a fixed C_o increases the quantity of surfactant adsorbed onto the interface. Therefore, $\tilde{\Gamma}_{eq}$ will increase with St_a. To understand how this change in $\tilde{\Gamma}_{eq}$ affects the equation of state, consider figure 3 where $El = 0.5$ and $\tilde{\Gamma}_{eq} = 0.2, 0.5, 0.8$. As $\tilde{\Gamma}_{eq}$ is increased, the equations of state shift upward and the equilibrium point (i.e. where $\gamma = \gamma^*/\gamma_{eq} = 1$) shifts to the right and moves closer to the singularity. Thus, the increase in $\tilde{\Gamma}_{eq}$ results in an increase in the slope of the equation of state, $\mathrm{d}\gamma/\mathrm{d}\Gamma$, near $\tilde{\Gamma}_{eq}$. So, by allowing $\tilde{\Gamma}_{eq}$ to change we are effectively changing the strength of the surfactant as a function of the adsorption depth and/or the sorption rates.

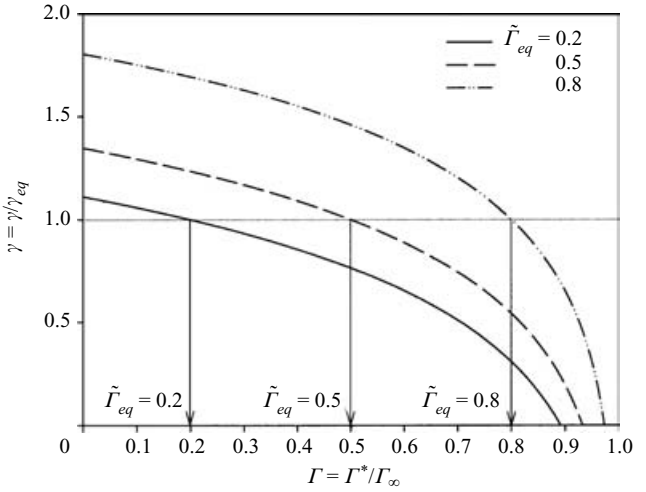

FIGURE 3. Dimensionless Langmuir equations of state at $El = 0.5$ and $\Gamma_{eq} = 0.2, 0.5, 0.8$. This figure demonstrates the change in relative surfactant strength ($d\gamma/d\Gamma$ at $\gamma = 1$) that can occur due to changes in the equilibrium point.

Dimensionless parameter	Definition	Description
Capillary number	$Ca = \mu U/\gamma_{eq}$	Relates viscous to surface tension forces
Bulk Péclet number	$Pe = UR/D_{mol}$	Relates bulk convection rates to diffusion rates
Surface Péclet number	$Pe_s = UR/D_{int}$	Relates surface convection rates to diffusion rates
Adsorption Stanton number	$St_a = k_a\Gamma_\infty/U$	Relates adsorption rates to surface convection rates
Desorption Stanton number	$St_d = k_d R/U$	Relates desorption rates to surface convection rates
Adsorption depth	$\lambda = \Gamma_\infty/C_o R$	Depth of fluid required to bring Γ to Γ_∞
Elasticity number	$El = \mathbb{R}T\Gamma_\infty/\gamma_{eq}$	Ability of surfactant to modify the surface tension

TABLE 1. Independent dimensionless physicochemical hydrodynamics parameters.

In contrast, we wish to gain a further understanding of this system by independently examining the effects of λ, St_a, and St_d without altering the surfactant strength. This can be accomplished by fixing the equilibrium point, $\tilde{\Gamma}_{eq}$, and thus prescribing the equation of state. In order to maintain a constant $\tilde{\Gamma}_{eq}$, two of the independent parameters (λ, St_a, and St_d) must be varied simultaneously. For example, if we increase the adsorption rate (St_a), equation (2.27) indicates that we must concurrently increase the desorption rate (St_d) to maintain a fixed equilibrium point. Simulations with a constant $\tilde{\Gamma}_{eq}$ are conducted in § 3.3 and § 3.4.2 and are termed 'fixed equilibrium point' studies. We will demonstrate that 'fixed equilibrium' and 'variable equilibrium' point simulations demonstrate strikingly different behaviour.

3. Results

The scaling analysis presented above yields the physicochemical hydrodynamic dimensionless parameters tabulated in table 1. Note that in addition to these independent parameters there are two additional dependent parameters: the effective adsorption parameter, $St_\lambda = St_a/\lambda$ and the dimensionless equilibrium point, $\tilde{\Gamma}_{eq}$. The goal of this paper is to vary these parameters separately to understand how different physicochemical properties can affect the mechanical properties of the system.

For each parameter variation study, the following set of parameters is used as the base conditions: $Ca = 0.15$, $El = 0.5$, $St_a = 1$, $St_d = 5$, $\lambda = 0.1$, $Pe = 10$, $Pe_s = 10^3$. The bulk concentration field for this base state is given by figure 12(*b*). At these parameter values, the transport of the surfactant due to bulk transport and surface adsorption/desorption processes are both $O(1)$. As a result, the equations governing bulk and surface transport cannot be simplified and the full set of non-linear governing equations must be solved. As shown below, the base parameter case as well as a large set of parameter variation studies can be accurately simulated with the current theoretical model. Therefore, this model has distinct advantages over previous models that can only simulate bulk-equilibrium or diffusion-limited conditions.

In exploring a given parameter, we provide several sets of multi-part figures to demonstrate the response of the system. For each parameter, first we provide a four-part figure that describes the variation of the following basic characteristics as a function of the parameter:

(*a*) dimensionless interfacial pressure drop at the tip, $\Pi_{tip} = P^*_{tip}/(\gamma_{eq}/R)$;
(*b*) dimensionless bubble width, $\beta_f = R_f/R$,
(*c*) surface tension component of Π_{tip}, $\gamma^*_{tip}\kappa_{tip}$,
(*d*) viscous component of Π_{tip}, $4Ca^*\mathrm{d}u_s/\mathrm{d}s_{tip}$.

Then, to explain the geometric and surface transport responses, an additional four-part figure is provided to demonstrate the variation in the following dimensionless surface variables:

(*a*) surface velocity, $u_s = u^*_s/U$;
(*b*) surface concentration, $\Gamma = \Gamma^*/\Gamma_\infty$;
(*c*) surface tension, $\gamma = \gamma^*/\gamma_{eq}$,
(*d*) subsurface surfactant concentration, $C_s = C^*_s/C_o$.

Through examination of these data will explain the relationships that develop in this complex system.

3.1. *Influence of Marangoni stress*

In this section we investigate the influence of the Marangoni stress parameter (Ma). Recall that $Ma = El/Ca = \mathbb{R}T\Gamma_\infty/\mu U$ is a ratio of Marangoni to viscous forces. We alter this parameter by varying either the capillary number (Ca), which is a ratio of viscous to surface tension forces, or by varying the elasticity number (El), which represents the ability of adsorbed surfactant to modify the interfacial surface tension.

3.1.1. *Variation of Ca*

In figure 4 we present the variation of the dimensionless (*a*) bubble tip pressure drop, (*b*) finger width, (*c*) surface tension component, and (*d*) viscous component as a function of Ca for fixed El values. Note that we have used two values for El other than the base parameter value of $El = 0.5$: $El = 0$ to simulate a passive surfactant that does not modify the surface tension (also a surfactant-free system) and $El = 1.0$ to simulate a more active surfactant. In both the passive and active surfactant systems, Π_{tip} increases with Ca. As El is increased, the Π_{tip} (Ca) curves shift upwards due primarily to an increase in the surface tension component, $\gamma_{tip}\kappa_{tip}$. Although γ_{tip} exhibits a non-monotonic relationship with Ca at large El (see figure 5*c* and description below), the surface tension component of Π_{tip} ($\gamma_{tip}\kappa_{tip}$ in figure 4*c*) increases monotonically with Ca. The β_f data at $El = 0$ (figure 4*b*) can

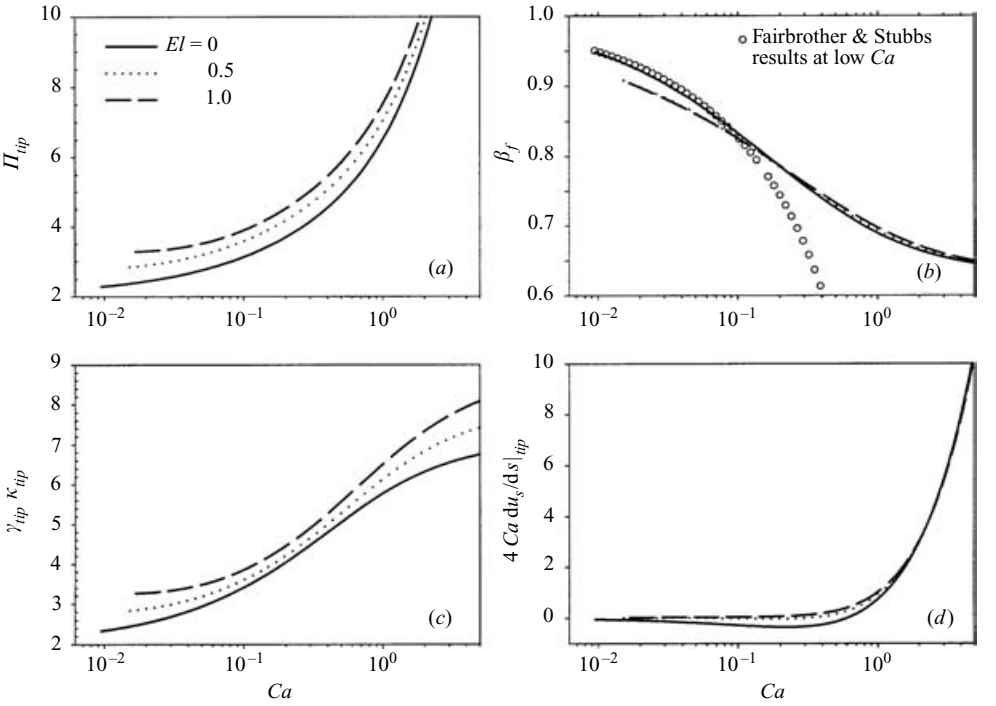

FIGURE 4. The influence of the capillary number (Ca) on the dimensionless (a) bubble tip pressure drop, (b) finger width, (c) surface tension component, and (d) viscous component. $El = 0, 0.5, 1.0$ ($St_a = 1$, $St_d = 5$, $\lambda = 0.1$, $Pe = 10$, $Pe_s = 10^3$).

be compared with previous studies to further validate the code. First, for $Ca < 0.1$ the current results are within 1% of the low-Ca measurements of Fairbrother & Stubbs (1935) (open circles in figure 4b). In addition, the β_f value at $Ca \sim 2$ (i.e. 0.67) is consistent with the high-Ca asymptote measured by Taylor (1961). Therefore, the current computational method predicts the well-established low- and high-Ca measurements for a surfactant-free system.

Figure 5 demonstrates how the dimensionless (a) surface velocity, (b) surface concentration, (c) surface tension, and (d) sub-surface concentration along the interface (defined by the arclength parameter, s) vary as a function of Ca for $El = 0.5$. Figure 5(c) indicates that for decreasing Ca, the tip surface tension, γ_{tip}, initially decreases to ~ 1.01 and then increases to ~ 1.10. To understand this non-monotonic relationship, consider the distribution of Γ and C_s demonstrated in figure 5(b, d). As Ca decreases, C_s in the thin film decreases due to transport limitations within the bulk phase. This occurs because the film becomes exceedingly thin ($1 - \beta_f \to 0$) as Ca is reduced and this leads to a very small volume of bulk surfactant being convected into the thin-film region. This depletion of surfactant in the thin film region as β_f increases is also consistent with the mass balance relationships developed in § 2.5. This reduction in C_s results in reduced surfactant adsorption and thus a reduction in the thin-film surface concentration, Γ_{film}. In fact, as the film thickness becomes of similar magnitude to the adsorption thickness (λ), the bulk surfactant delivered to the thin-film region is too small for the interface to reach $\tilde{\Gamma}_{eq}$, as discussed in Ghadiali *et al.* (2001). So, at small Ca the transport from the bulk to the interface in the thin-film region results in very small values of Γ_{film}. In contrast, Γ near the

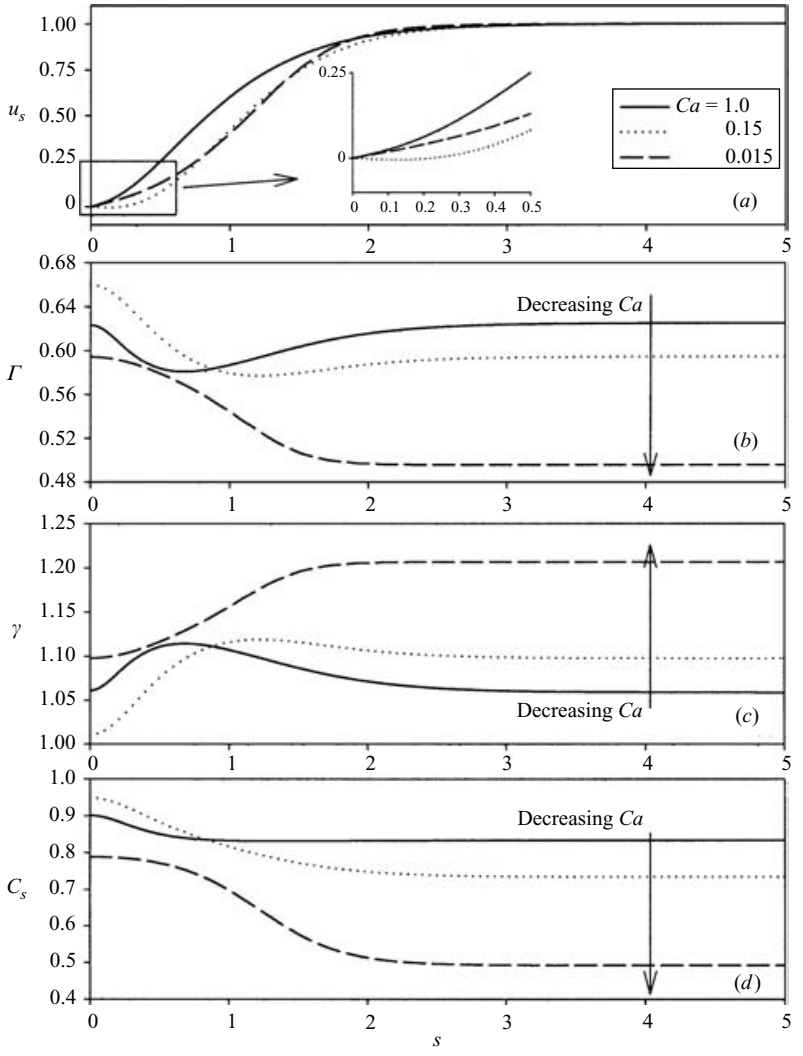

FIGURE 5. The influence of the capillary number (Ca) on the dimensionless (a) surface velocity, (b) surface concentration, (c) surface tension, and (d) sub-surface concentration along the interface for $Ca = 1.0, 0.15, 0.015$ ($El = 0.5$, $St_a = 1$, $St_d = 5$, $\lambda = 0.1$, $Pe = 10$, $Pe_s = 10^3$).

bubble tip (Γ_{tip}) deviates from Γ_{film} due to surface convection patterns near the tip. As Ca is reduced from 1.0 to 0.15 a recirculation zone develops at the bubble tip. This can be seen by the inset of figure 5(a), where u_s becomes negative in the tip region at $Ca = 0.15$. As a result of retrograde surface convection, Γ_{tip} increases as Ca decreases over the range $0.15 \leqslant Ca \leqslant 1.0$ as shown in figure 5(b). However at sufficiently low Ca, $Ma = El/Ca$ becomes large enough that Marangoni stresses move the recirculation region away from the interface tip (u_s is no longer negative in the tip region) and the transport limitations in the thin film decrease Γ_{film} significantly. As a result, Γ_{tip} decreases as Ca decreases over the range $0.015 \leqslant Ca \leqslant 0.15$. Since γ is inversely related to Γ, γ_{tip} depicted figure 5(c) exhibits the opposite behaviour, where γ_{tip} initially decreases and then increases as Ca is reduced.

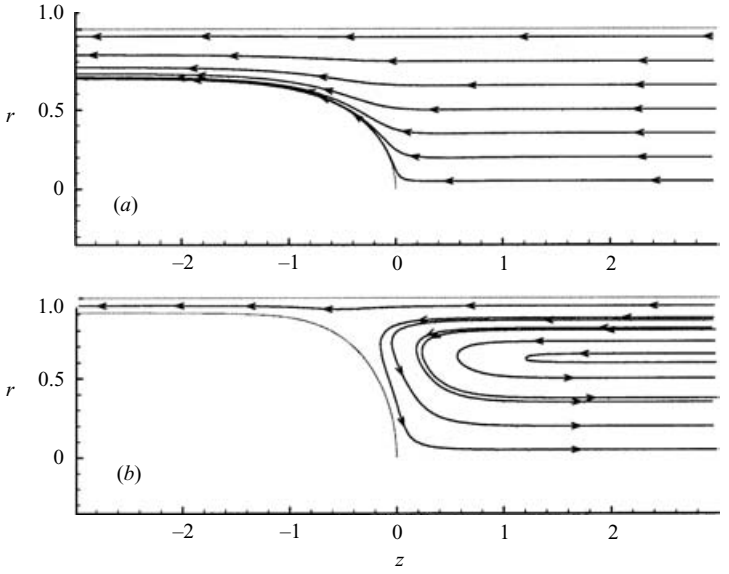

FIGURE 6. Streamlines surrounding the semi-infinite bubble for (*a*) $Ca = 1.0$ and (*b*) 0.015 ($El = 0.5$, $St_a = 1$, $St_d = 5$, $\lambda = 0.1$, $Pe = 10$, $Pe_s = 10^3$).

Figure 6 shows the flow field surrounding the semi-infinite air bubble for large ($Ca = 1.0$) and small ($Ca = 0.015$) capillary numbers. The streamlines are drawn in a bubble-tip reference frame. At large Ca, the film thickness is relatively large (small β_f) and the fluid flows around the bubble unidirectionally. However, at small Ca the upstream fluid thickness becomes very small ($1 - \beta_f \rightarrow 0$), so the fluid approaching the bubble must change direction, forming a bulk recirculation profile. Although this recirculating flow field exists in the bulk, figure 5(*a*) indicates that for $Ca = 0.015$ and $El = 0.5$ the surface velocities are unidirectional (i.e. all positive u_s). As discussed in detail in § 3.1.2, Marangoni stresses (which are relatively large in this case, $Ma = El/Ca = 33.3$) rigidify the interface and move the recirculating flow pattern away from the interface. As a result, the recirculating flow is confined to the bulk.

3.1.2. *Variation of El*

Figure 7 demonstrates the variation in system variables as a function of El for a fixed $Ca = 0.15$. Figure 7(*a*) demonstrates a monotonic increase in Π_{tip} with increasing El, primarily due to an increase in the surface tension component, $\gamma_{tip}\kappa_{tip}$. In addition, as El increases, the viscous component of Π_{tip} ($4\,Ca\,\mathrm{d}u_s/\mathrm{d}s|_{tip}$) also increases (figure 7*d*) due to an increase in the velocity gradient at the tip, $\mathrm{d}u_s/\mathrm{d}s|_{tip}$ (see figure 8*a* and corresponding description below). Note that the dotted horizontal lines in figure 7 indicate the equilibrium values that would be observed if $\gamma = \gamma_{eq}$ uniformly. As $El \rightarrow 0$, surfactants do not modify the surface tension and thus γ is constant and all system variables approach equilibrium values.

Figure 8 demonstrates the variation in the surface variables as a function of interfacial position for $El = 10^{-3}$, 0.49, 2.05. As El increases, the magnitude of $\mathrm{d}\gamma/\mathrm{d}s$ near the bubble tip increases (figure 8*c*) even though $\mathrm{d}\Gamma/\mathrm{d}s$ decreases (figure 8*b*). Therefore, at large El the Marangoni stress, τ_M, drives the bulk recirculating flow pattern away from the interface (see figure 9 for details). As a result, the negative

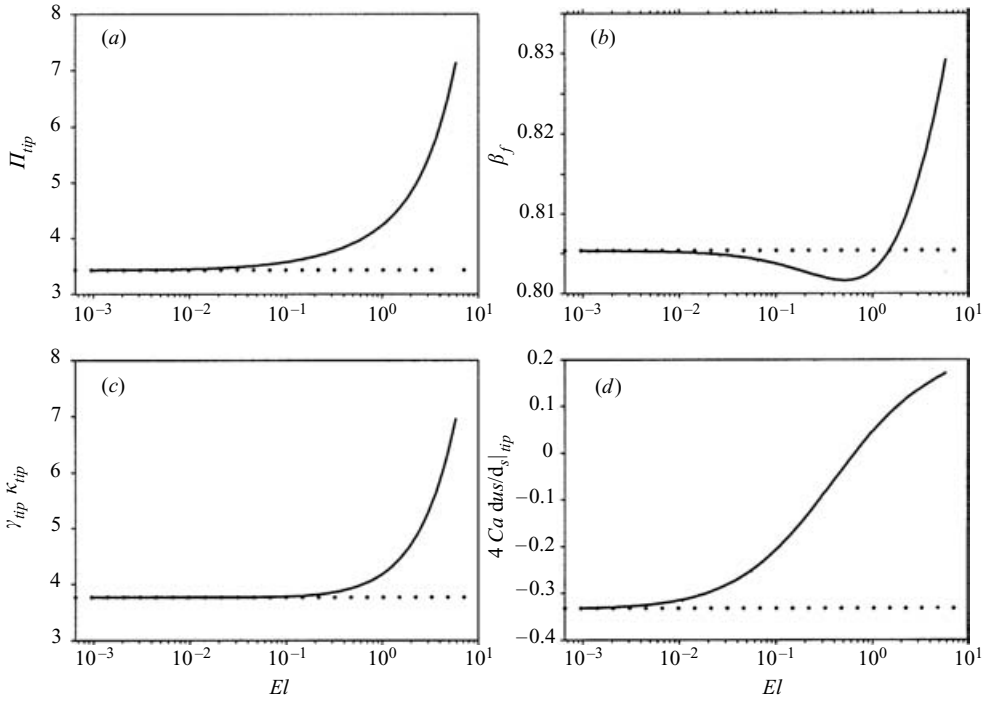

FIGURE 7. The influence of the elasticity parameter (El) on the dimensionless (a) bubble tip pressure, (b) finger width, (c) surface tension component, and (d) viscous component ($Ca = 0.15$, $St_a = 1$, $St_d = 5$, $\lambda = 0.1$, $Pe = 10$, $Pe_s = 10^3$). Dotted horizontal lines indicates behaviour that would occur if $\gamma = \gamma_{eq}$ uniformly.

u_s values observed at low El are eliminated and the slope ($\mathrm{d}u_s/\mathrm{d}s|_{tip}$) increases with increasing El (figure 8a).

The surface tension profiles shown in figure 8(c) can also be used to understand the non-monotonic behaviour in β_f shown in figure 7(b). β_f is determined by the magnitude of two effects – the Marangoni stress (τ_M), and the average thin film surface tension (γ_{film}). Recall that τ_M is directed from regions of low γ to regions of high γ. Therefore, as shown in figure 8(c), τ_M is predominately directed from the tip to the thin film. As a result, fluid is driven into the thin film causing the film to thicken (reduction in β_f). This decrease in β_f with increasing El is initially observed at low El values (figure 7b). However, a further increase in El results in a larger γ_{film} (figure 8c) and thus a decrease in the thin-film capillary number, $Ca_{film} = \mu U/\gamma_{film}$. The increase in β_f (film thinning) at larger El is thus due to a relative decrease in viscous to surface tension forces (figure 7b).

Figure 9 demonstrates the influence of τ_M on the bulk recirculating flow field. At small $El(= 10^{-3})$, the interface is mobile and does not support a significant Marangoni stress. Under these conditions, the bulk recirculating flow is in contact with the interface and the surface velocity (u_s) can take on negative values near the tip (figure 8a). As El increases, surface tension gradients generate a τ_M that opposes the basis flow field and begins to rigidify the interface. At large El (= 5.13), τ_M has forced the bulk recirculating flow pattern away from the interface such that the surface velocities are all positive. This change in the bulk flow field will influence the quantity of surfactant that can be transported to the interface via bulk convection.

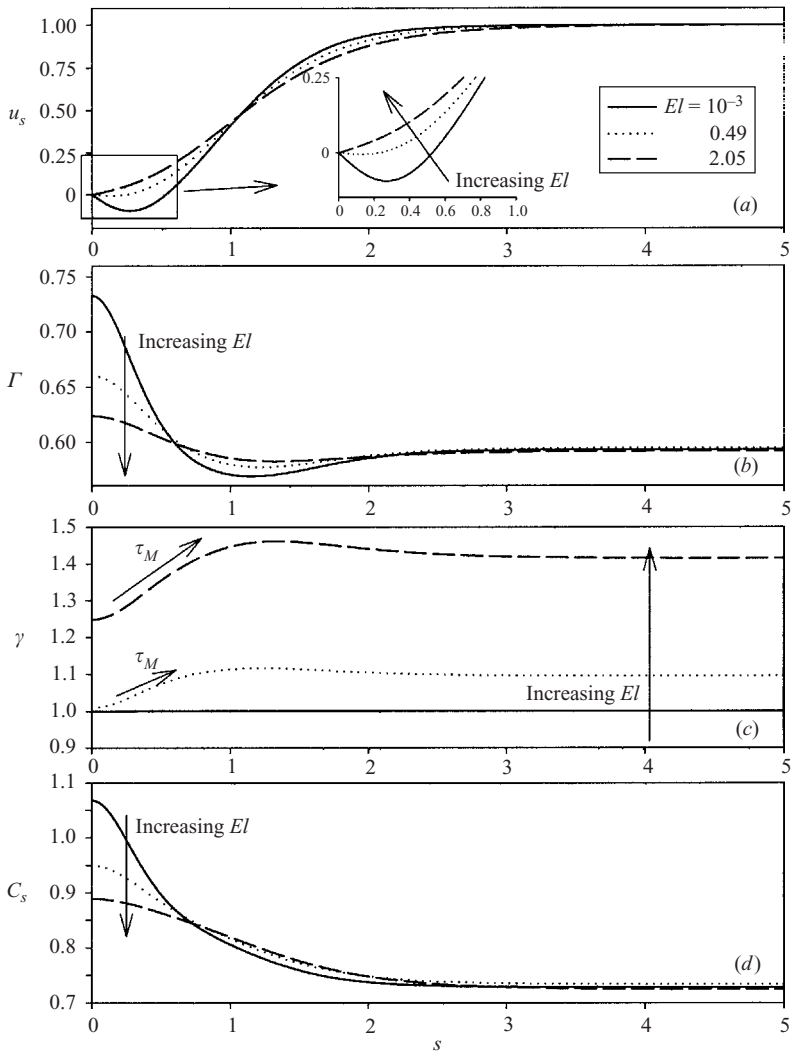

FIGURE 8. The influence of El on the dimensionless (a) surface velocity, (b) surface concentration, (c) surface tension, and (d) sub-surface concentration along the interface for $El = 10^{-3}, 0.49, 2.05$ ($Ca = 0.15$, $St_a = 1$, $St_d = 5$, $\lambda = 0.1$, $Pe = 10$, $Pe_s = 10^3$).

3.2. *Influence of bulk diffusion*

To investigate the influence of the bulk diffusion rate we independently varied Pe while holding all other transport parameters constant under low and high concentrations ($\lambda = 0.1$ and $\lambda = 0.01$, respectively). Figure 10 shows the variation in system variables as a function of Pe. For $\lambda = 0.1$, Π_{tip} exhibits a non-monotonic response to an increase in Pe where, Π_{tip} decreases slightly at small Pe before increasing at larger Pe. As demonstrated in figure 10(c, d), the change in the viscous component of Π_{tip} is negligible compared to the change in the surface tension component, $\gamma_{tip}\kappa_{tip}$.

Figure 10 also demonstrates the variation in system variables with Pe at a large bulk concentration ($\lambda = 0.01$). For this simulation we have fixed the effective adsorption rate ($St_\lambda = 10$) by setting $St_a = 0.1$ such that the equilibrium point is fixed (see § 3.4.2 for details). $\lambda \ll 1$ corresponds to a large bulk concentration, where the transport of

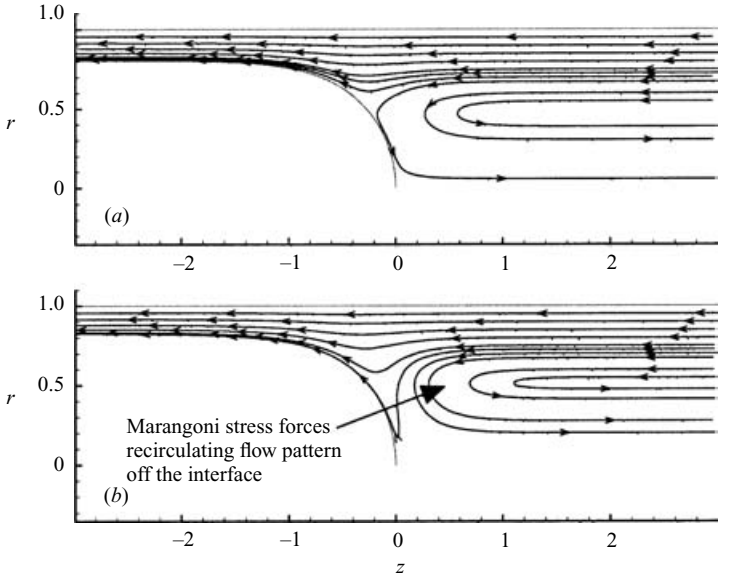

FIGURE 9. Streamlines surrounding the semi-infinite bubble for (*a*) $El = 10^{-3}$ and (*b*) 5.13 ($Ca = 0.15$, $St_a = 1$, $St_d = 5$, $\lambda = 0.1$, $Pe = 10$, $Pe_s = 10^3$). The arrow at $El = 5.13$ indicates the removal of the recirculating flow pattern from the interface.

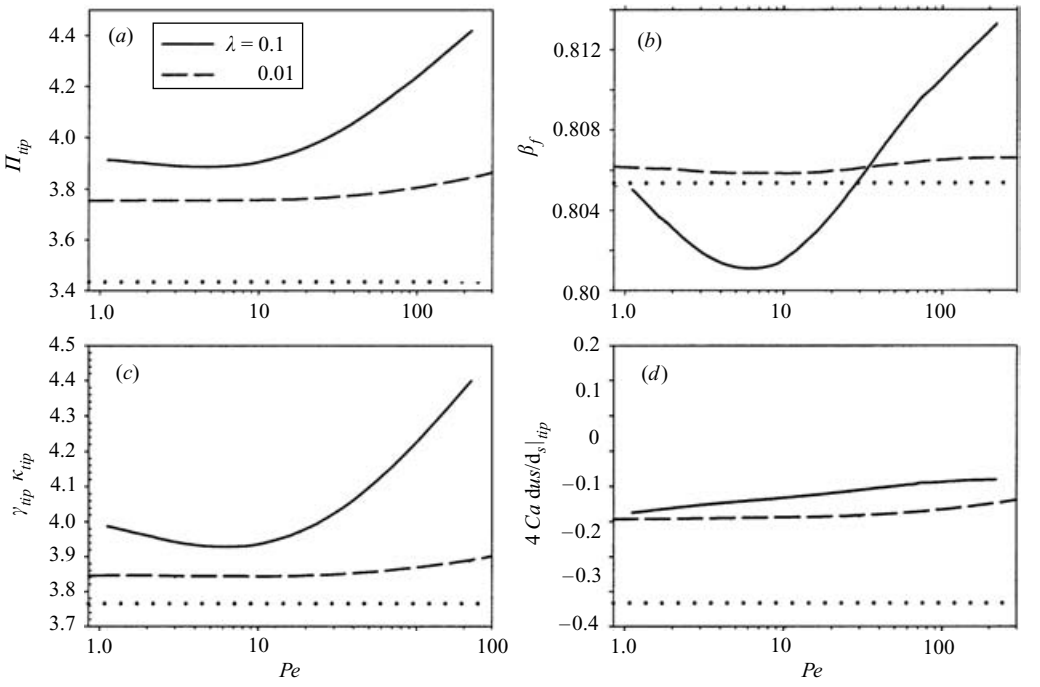

FIGURE 10. The influence of the bulk Peclet number (Pe) on the dimensionless (*a*) bubble tip pressure, (*b*) finger width, (*c*) surface tension component, and (*d*) viscous component for $\lambda = 0.1$, $St_a = 1$ and $\lambda = 0.01$, $St_a = 0.1$ ($Ca = 0.15$, $El = 0.5$, $St_d = 5$, $Pe_s = 10^3$). Dotted horizontal lines indicate equilibrium values if $\gamma = \gamma_{eq}$ uniformly.

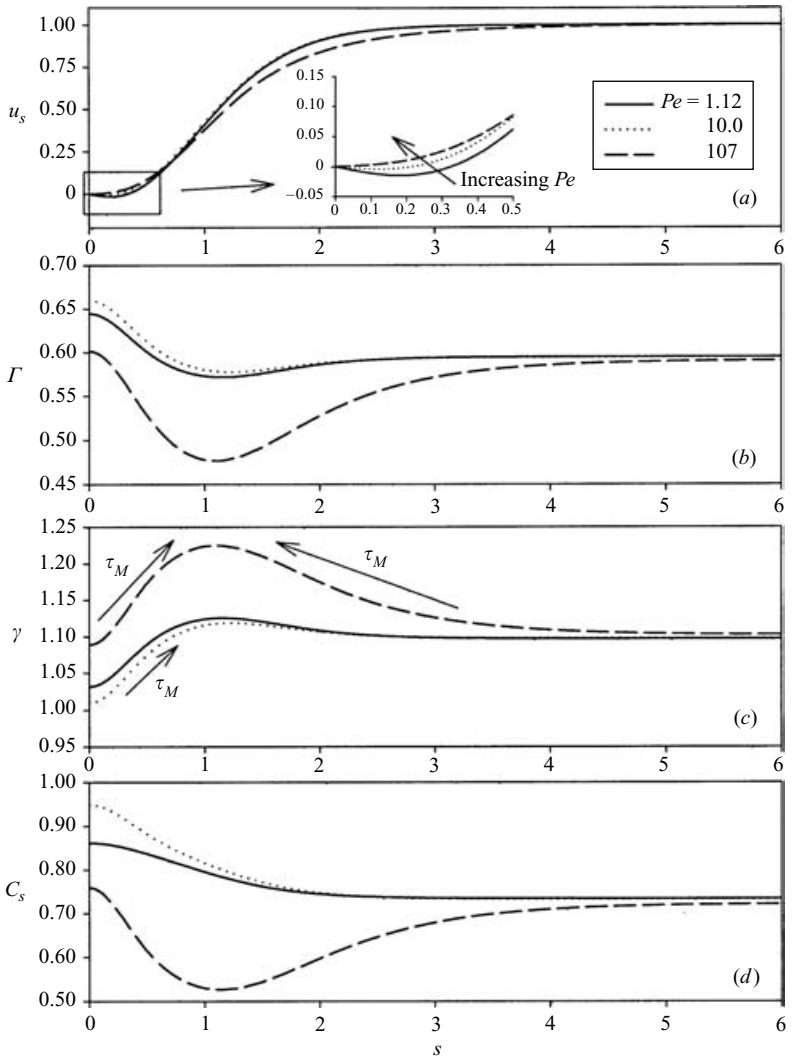

FIGURE 11. The influence of Pe on the dimensionless (a) surface velocity, (b) surface concentration, (c) surface tension, and (d) sub-surface concentration along the interface for $Pe = 1.12, 10.0, 107$ ($Ca = 0.15$, $El = 0.5$, $St_a = 1$, $St_d = 5$, $\lambda = 0.1$, $Pe_s = 10^3$).

surfactant in the bulk is rapid, leading to a uniform bulk concentration that is nearly equal to the far-field value, C_o. Therefore, the large bulk concentration gradients that develop at large Pe for $\lambda = 0.1$ (see figure 12) are not generated at $\lambda = 0.01$. As a result, the system variables, including Π_{tip}, are significantly less sensitive to changes in Pe. In addition, at $\lambda = 0.1$, the bulk transport limitation ($C_s \neq 1$) prevents the system variables from approaching the equilibrium values as indicated in figure 10. As λ decreases, the bulk transport limitation is reduced ($C_s \rightarrow 1$), and thus the system variables are closer to the equilibrium values. However, even at $\lambda = 0.01$, the moderate effective adsorption rate, $St_\lambda = 10$, prevents the system variables from obtaining the equilibrium values that would occur if $\gamma = \gamma_{eq}$ uniformly.

Figure 11 shows the variation in the surface variables as a function of interfacial position for $Pe = 1.12,\ 10.0,\ 107$ and $\lambda = 0.1$. Consider the distribution of C_s shown

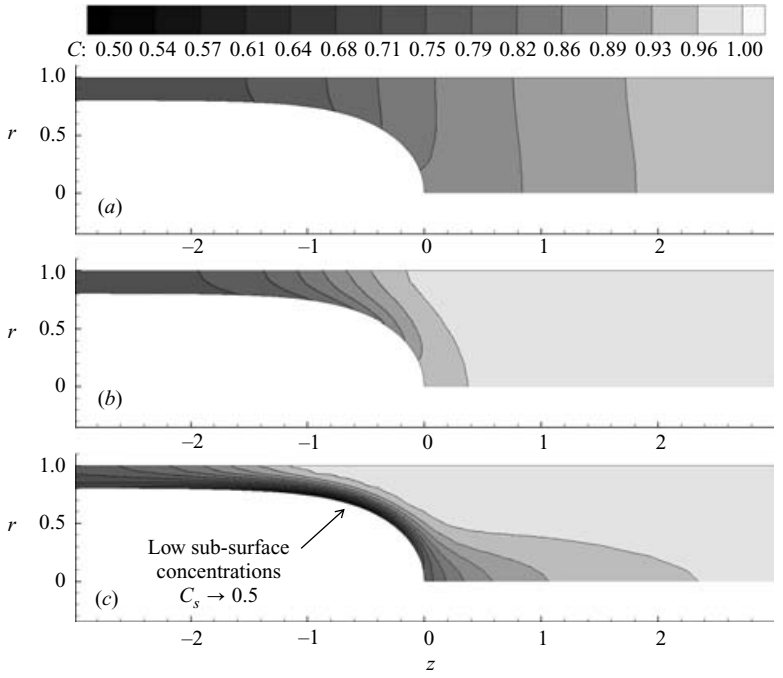

FIGURE 12. Bulk concentration field surrounding the semi-infinite bubble for (*a*) $Pe = 1.12$, (*b*) 10.0, (*c*) 107 ($Ca = 0.15$, $El = 0.5$, $St_a = 1$, $St_d = 5$, $\lambda = 0.1$, $Pe_s = 10^3$).

in figure 11(*d*). Although the thin film concentration, $C_{s,film}$, is largely independent of Pe, large concentration gradients develop in the bulk fluid as Pe increases, which alters the magnitude of C_s near the bubble tip (see figure 12). At low Pe ($Pe = 1.12$), the recirculating flow pattern (see inset in figure 11*a*) convects surfactant to the tip and results in an increase in the tip value of C_s over that in the thin film. However, as Pe increases further ($Pe = 107$), diffusion limitations lower the average C_s value while gradients in Γ (and thus γ) reduce the recirculating flow pattern at the interface and thereby further reduce C_s near the tip. Since sorption of Γ is governed by the local C_s, Γ_{tip} (and therefore γ_{tip}) also displays this non-monotonic behaviour (figure 11*b*, *c*).

The surface tension profile (figure 11*c*) can also be used to explain the non-monotonic behaviour of β_f (figure 10*b*). For $Pe = 10$, the magnitude of the Marangoni stress, τ_M, is directed toward the thin film and results in film thickening. However, when $Pe > 10$, the surfactant distribution creates a bi-directional Marangoni stress field where τ_M near the tip is directed towards the thin film while τ_M near the thin film is directed towards the tip. So, at large Pe the Marangoni stress in the thin-film region drives fluid out of the thin film and results in a film thinning response for $Pe > 10$.

Figure 12 shows the bulk concentration field surrounding the semi-infinite bubble at $Pe = 1.12$, 10.0, 107. Recall that we have specified a continuity between the bulk diffusive and the adsorptive/desorptive fluxes at the interface (2.19). For an $O(1)$ adsorptive/desorptive flux, equation (2.19) indicates that at low Pe (or high D_{mol}) the concentration gradients near the interface $\mathrm{d}C/\mathrm{d}\hat{\boldsymbol{n}}$ must be small, as demonstrated in figure 12(*a*) for $Pe = 1.12$. As Pe increases, $\mathrm{d}C/\mathrm{d}\hat{\boldsymbol{n}}$ becomes larger as convection begins to dominate transport. As a result, $\mathrm{d}C/\mathrm{d}\hat{\boldsymbol{n}}$ increases as demonstrated in figure 12(*c*)

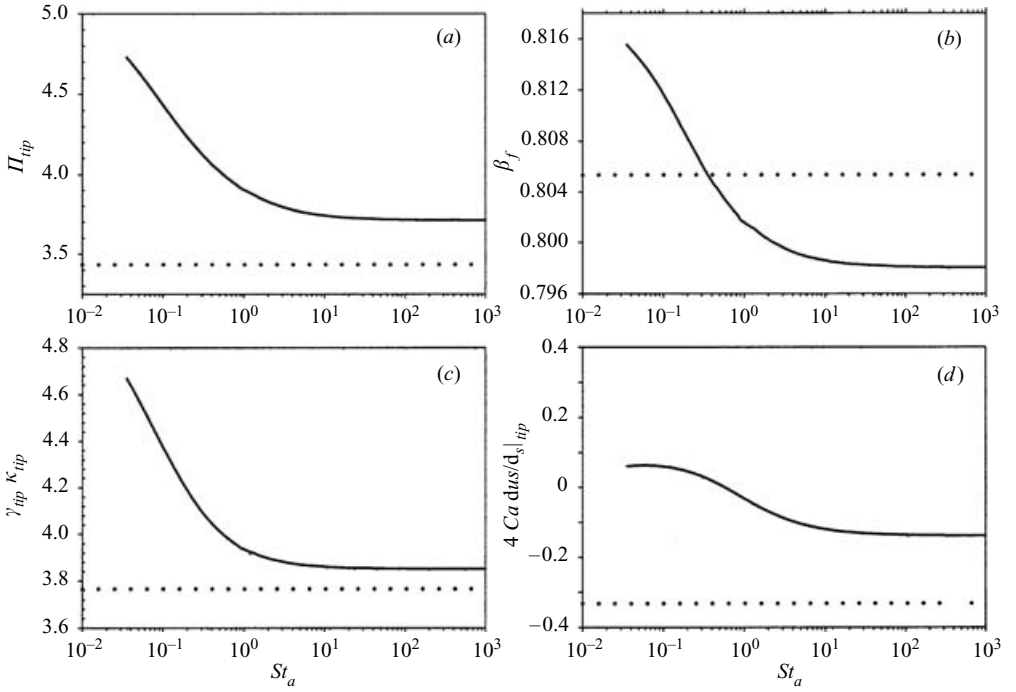

FIGURE 13. The influence of St_a at constant $\tilde{\Gamma}_{eq}$ on the dimensionless (a) bubble tip pressure, (b) finger width, (c) surface tension component and (d) viscous component. ($St_d = St_\lambda(1-\tilde{\Gamma}_{eq})/\tilde{\Gamma}_{eq}$, $Ca = 0.15$, $El = 0.5$, $\lambda = 0.1$, $Pe = 10$, $Pe_s = 10^3$). Dotted horizontal lines indicate equilibrium values that would occur if $\gamma = \gamma_{eq}$ uniformly.

for $Pe = 107$. At very large Pe, the generation of a very large $\mathrm{d}C/\mathrm{d}\hat{\boldsymbol{n}}$ results in sub-surface concentrations within the transition region that are less than the thin-film value (figure 11d), causing an increase in γ in the transition region. As discussed above, this results in a film-thinning response.

3.3. *Influence of adsorption/desorption kinetics*

In order to isolate the effect of surfactant sorption properties, we conducted a fixed equilibrium point study that maintains a fixed surfactant strength by varying St_a and St_d simultaneously so that $\tilde{\Gamma}_{eq}$ remains constant (see § 2.7). As such, every variation in St_a is accompanied by a change in St_d so that $St_d = St_\lambda(1-\tilde{\Gamma}_{eq})/\tilde{\Gamma}_{eq}$. Under these conditions, an increase or decrease in St_a can be interpreted as an increase or decrease in the surfactant sorption properties at a fixed surfactant strength or equilibrium point.

Figure 13 shows the variation in system variables as a function of St_a for a constant $\tilde{\Gamma}_{eq}$. As St_a decreases, Π_{tip} increases monotonically. This increase in Π_{tip} is due to an increase in surface tension component (figure 13c) as well as a more modest increase in the viscous component (figure 13d). As St_a increases for-fixed $\tilde{\Gamma}_{eq}$, Γ equilibrates with the local C_s. However, as shown in figure 14(d), bulk transport limitation still exists ($C_s < 1$) since $\lambda = 0.1$. As a result, the system variables do not approach equilibrium values at large St_a.

To understand the increase in the surface tension and viscous components that occur with a reduction St_a, consider the variation in the surface variables as a function of interfacial position for $St_a = 0.036$, 0.12, 99 (figure 14). At very large St_a,

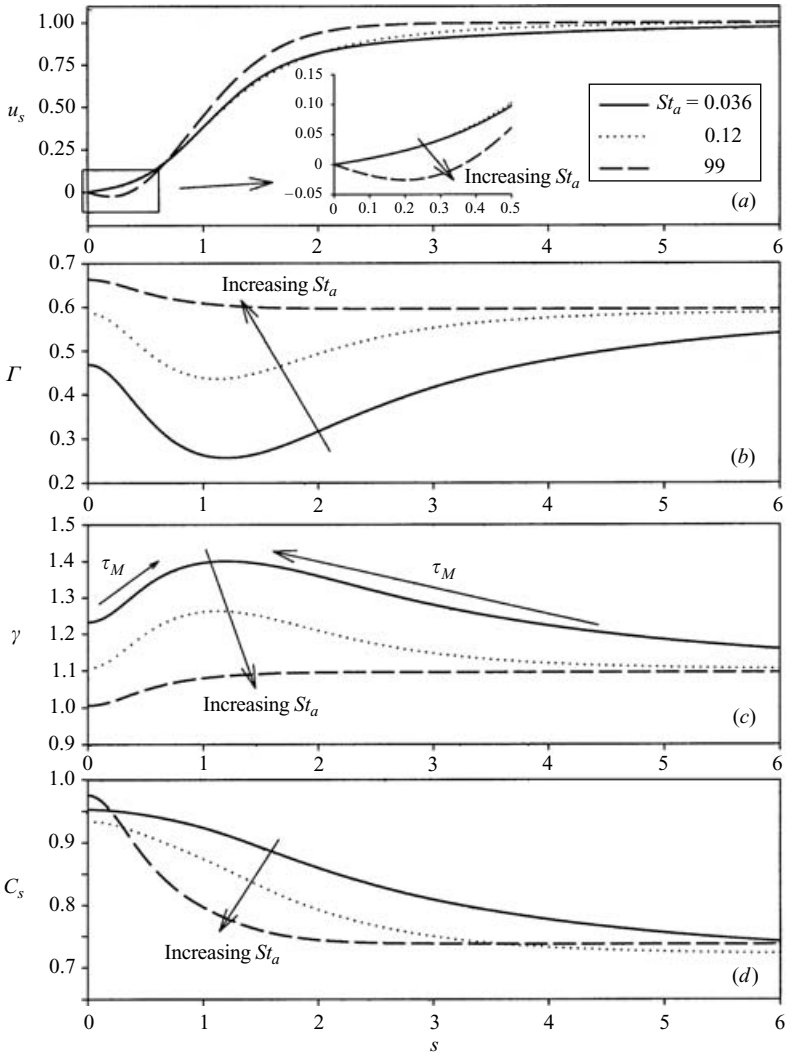

FIGURE 14. The influence of St_a at constant $\tilde{\Gamma}_{eq}$ on the dimensionless (*a*) surface velocity, (*b*) surface concentration, (*c*) surface tension, and (*d*) sub-surface concentration along the interface for $St_a = 0.036, 0.12, 99$. ($St_d = St_\lambda(1-\tilde{\Gamma}_{eq})/\tilde{\Gamma}_{eq}$, $Ca = 0.15$, $El = 0.5$, $\lambda = 0.1$, $Pe = 10$, $Pe_s = 10^3$).

the surface concentration, Γ, is in equilibrium with the sub-surface concentration, C_s. As St_a decreases, surface convection depletes the surfactant on the interface more rapidly than adsorption can replenish the interface. As a result, at low St_a significant non-equilibrium surface concentrations and tensions can develop in the bubble-tip and thin-film regions, as shown in figure 14(*b*, *c*). Note that the computational domain is longer than that shown in figure 14 so that the equilibrium specified in § 2.6 is satisfied at small values of St_a. As St_a decreases, the depletion of surfactant at the bubble tip results in an increase in γ_{tip} and thus an increase in $\gamma_{tip}\kappa_{tip}$. In addition, as St_a decreases, the non-uniformity of γ near the bubble tip increases the magnitude of the τ_M near the bubble tip. This increase in τ_M rigidifies the interface and removes the recirculating flow pattern from the interface as demonstrated in figure 14(*a*). As a

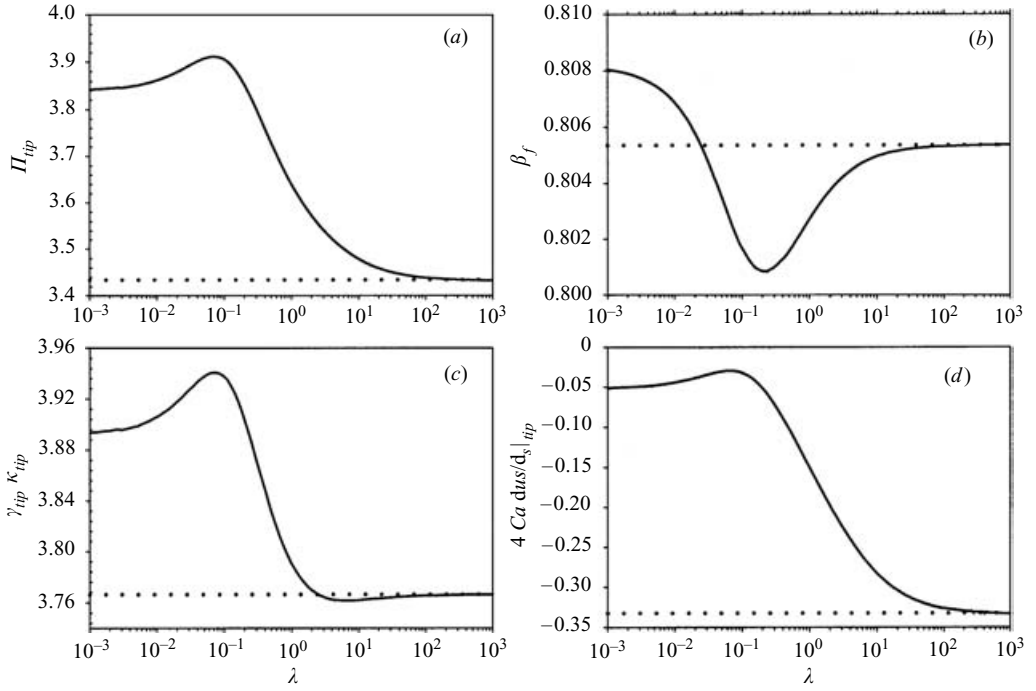

FIGURE 15. The influence of λ at a variable $\tilde{\Gamma}_{eq}$ on the dimensionless (a) bubble tip pressure, (b) finger width, (c) surface tension component, and (d) viscous component. ($\tilde{\Gamma}_{eq} = St_\lambda/(St_\lambda + St_d)$, $Ca = 0.15$, $El = 0.5$, $St_a = 1$, $St_d = 5$, $Pe = 10$, $Pe_s = 10^3$). Dotted horizontal lines indicate equilibrium values when $\gamma = \gamma_{eq}$ uniformly.

result, the magnitude of $\mathrm{d}u_s/\mathrm{d}s|_{tip}$, and thus the viscous component of Π_{tip}, increases as St_a decreases. Finally, an elevated γ in the transition region generates a large Marangoni stress that is directed away from the thin film and thus results in film thinning (increase in β_f) at low St_a (figure 13b).

3.4. *Influence of adsorption depth*

3.4.1. *Variation of λ – variable equilibrium point*

In this section, the influence of the adsorption depth is investigated by varying λ and allowing $\tilde{\Gamma}_{eq}$ to vary simultaneously. This analysis is consistent with modification of the bulk concentration, C_o with $\lambda = \Gamma_\infty/(C_o R)$ and $St_\lambda = k_a C_o R/U$. Since St_λ increases with C_o, an increase in $\tilde{\Gamma}_{eq}$ results. This, in turn, leads to amplification of the Marangoni effect because the slope of the equation of state is a function of $\tilde{\Gamma}_{eq}$.

As demonstrated in figure 15(a), Π_{tip} exhibits an interesting non-monotonic behaviour as a function of λ. At large λ, concentrations are small, which causes $\tilde{\Gamma}_{eq} \ll 1$. This results in very small Marangoni stresses because $\mathrm{d}\gamma/\mathrm{d}\Gamma \ll 1$ (figure 3). Therefore, as λ becomes very large, $C_o \to 0$, $\Gamma \to 0$ and $\gamma \to \gamma_{clean}$. As a result, the system variables approach equilibrium values at large λ. As λ decreases due to an increase in C_o, the dimensionless pressure drop $\Pi_{tip} = P^*_{tip}/(\gamma^*_{eq}/R)$ initially increases before decreasing slightly at very small λ. This non-monotonic response is due primarily to the surface tension component, $\gamma_{tip}\kappa_{tip}$ (figure 15c), which results from the non-monotonic behaviour of γ_{tip}. The viscous component exhibits a similar non-monotonic behaviour (figure 15d). It should be noted that although the dimensionless pressure, Π_{tip}, increases with decreasing λ, the dimensional pressure, P^*_{tip}, decreases

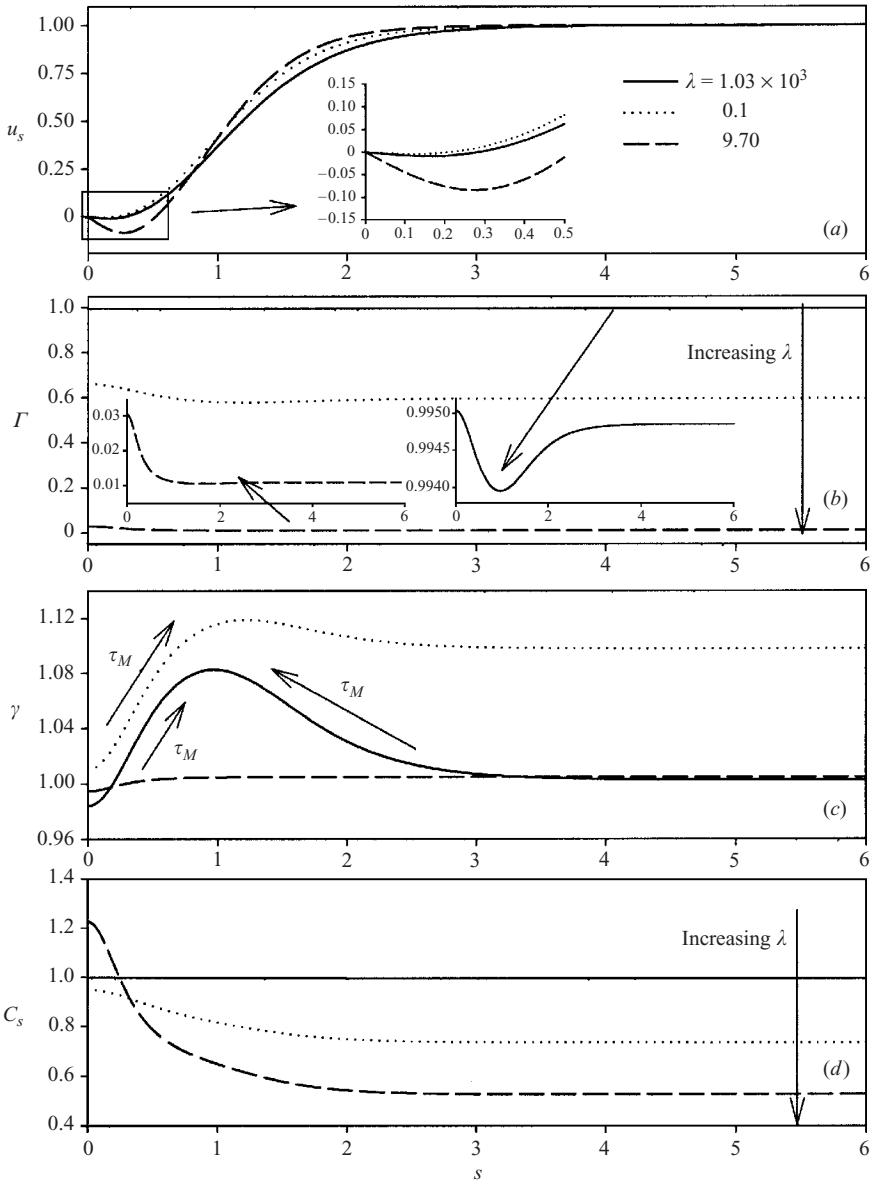

FIGURE 16. The influence of λ at a variable $\tilde{\Gamma}_{eq}$ on the dimensionless (*a*) surface velocity, (*b*) surface concentration, (*c*) surface tension, and (*d*) sub-surface concentration along the interface for $\lambda = 1.03 \times 10^{-3}, 0.1, 9.70$. $\tilde{\Gamma}_{eq} = St_\lambda/(St_\lambda + St_d)$, $Ca = 0.15$, $El = 0.5$, $St_a = 1$, $St_d = 5$, $Pe = 10$, $Pe_s = 10^3$.

with decreasing λ because more surfactant is adsorbed onto the interface as C_o increases (reducing γ^*_{eq}).

To understand the variations in surface tension and viscous components of Π_{tip}, we consider the concentration and surface tension profiles shown in figure 16 for $\lambda = 1.03 \times 10^{-3}$, 0.1, 9.70. At large λ, St_λ is very small and only a small quantity of surfactant can adsorb onto the interface. As a result, $\tilde{\Gamma}_{eq}$ is small and $\Gamma \ll 1$ for large λ as shown in figure 16(*b*). Under these conditions, the dimensionless surface

tension, figure 16(*c*), is nearly uniform and $\gamma \approx \gamma_{eq}$. As λ decreases, the magnitude of $\mathrm{d}\gamma/\mathrm{d}\Gamma$ increases due to an increase in $\tilde{\Gamma}_{eq}$ (see figure 3). Hence, small variations in Γ near $\tilde{\Gamma}_{eq} \sim 1$ produce large surface tension deviations from equilibriu!m as well as larger surface tension gradients. As λ decreases to $\lambda = 0.1$, γ_{tip} increases slightly and the Marangoni stress (τ_M) near the bubble tip also increases (figure 16*c*). The increase in γ_{tip} results in an initial increase in the surface tension component of Π_{tip}, while the increase in τ_M increases the viscous component via an increase in $\mathrm{d}u_s/\mathrm{d}s|_{tip}$ (figure 16*a*). As λ is decreased further to 1.03×10^{-3}, the concurrent increase in St_λ reduces the variations in Γ since the system approaches equilibrium at large adsorption rates. However, this decrease in λ is accompanied by an increase in $\tilde{\Gamma}_{eq}$ such that at very low λ, $\tilde{\Gamma}_{eq} \to 1$. Under these conditions, the singularity in the equation of state increases $\mathrm{d}\gamma/\mathrm{d}\Gamma$ so that significant variations in γ from γ_{eq} occur that result in responses that are far from equilibrium even though sorption rates are very rapid (see figure 3). As we will see below, this is very different from the response of the fixed-equilibrium system. It is interesting to note that the recirculating pattern is not completely removed from the interface (figure 16*a*) even for $\lambda \ll 1$, and therefore Γ can exceed $\tilde{\Gamma}_{eq}$ slightly at the tip (see inset to figure 16*b* where $\tilde{\Gamma}_{eq} = 0.9948$ for $\lambda = 1.03 \times 10^{-3}$). Therefore, for $\lambda = 1.03 \times 10^{-3}$, γ_{tip} can be reduced to $\gamma_{tip} < 1$ while the rest of the transition region exhibits $\gamma > 1$. This reduction in γ_{tip} decreases $\gamma_{tip}\kappa_{tip}$ and thus reduces Π_{tip} at very low λ.

The surface tension profiles (figure 16*c*) can also be used to understand the variation in β_f (figure 15*b*). As λ initially decreases, τ_M near the bubble tip is directed towards the thin film and results in film thickening (decrease in β_f). However, at very low λ the τ_M near the thin film (which is directed away from the thin film) begins to dominate and results in film thinning (increase in β_f).

3.4.2. *Variation of λ – fixed equilibrium point*

In this section we wish to investigate the influence of the adsorption depth for a fixed $\tilde{\Gamma}_{eq}$ value. To hold $\tilde{\Gamma}_{eq}$ constant, variations in λ are accompanied by modifications in St_a such that $St_a = \lambda St_d \tilde{\Gamma}_{eq}/(1 - \tilde{\Gamma}_{eq})$. Under these conditions, variations in λ are investigated at a fixed effective adsorption rate $St_\lambda = St_a/\lambda$ so that $\mathrm{d}\gamma/\mathrm{d}\Gamma$ at the equilibrium point is constant.

Figure 17 shows the variation in system variables as a function of λ for a constant $\tilde{\Gamma}_{eq}$. As λ increases, Π_{tip} increases monotonically. This increase in Π_{tip} is almost completely due to an increase the surface tension component (figure 17*c*). The viscous component exhibits a slightly non-monotonic behaviour (figure 17*d*), and the magnitude of this variation is significantly less that the surface tension component. As $\lambda \to 0$ for fixed $\tilde{\Gamma}_{eq}$, the bulk transport barrier is eliminated ($C_s = 1$) as shown in figure 18(*d*). However, the system remains adsorption-limited due to the fixed effective adsorption rate. As a result, the system variables do not reach their equilibrium values even at low λ.

To understand the increase in the surface tension component of Π_{tip} (figure 17*c*), consider the Γ and γ profiles for $\lambda = 1.03 \times 10^{-3}$, 0.99, 9.70 shown in figure 18. As λ increases, a significant decrease in Γ occurs along the entire interface. However, this reduction is far less significant than in the variable-equilibrium case (figure 16*b*) because of the simultaneous modification of the sorption rates that occur in this fixed-equilibrium study, holding $\tilde{\Gamma}_{eq}$ constant. So, global variation of Γ is far less pronounced than when $\tilde{\Gamma}_{eq}$ is allowed to vary (see § 3.4.1). Nevertheless, variation of Γ (figure 18*b*) has a significant impact on γ resulting in large Marangoni stresses at

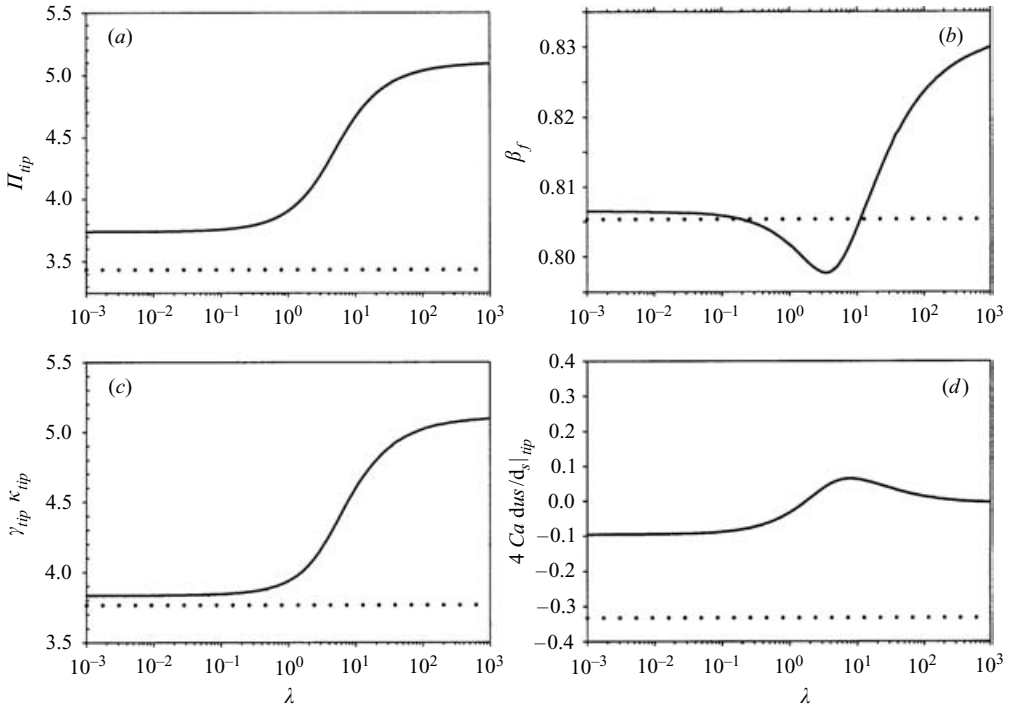

FIGURE 17. The influence of λ at a fixed $\tilde{\Gamma}_{eq}$ on the dimensionless (*a*) bubble tip pressure, (*b*) finger width, (*c*) surface tension component, and (*d*) viscous component. $St_a = \lambda St_d/(1-\tilde{\Gamma}_{eq})$, $Ca = 0.15$, $El = 0.5$, $St_d = 5$, $Pe = 10$, $Pe_s = 10^3$. Dotted horizontal lines indicate behaviour if $\gamma = \gamma_{eq}$ uniformly.

the tip (Figure 18*c*) that rigidify the interface and remove recirculation from the tip (figure 18*a*, inset).

The surface tension profile in figure 18(*c*) also explains the non-monotonic behaviour of β_f demonstrated in figure 17(*b*). For small λ, the Marangoni stress near the bubble tip is directed towards the thin film and results in film thickening (reduction of β_f). However, at large λ the thin-film surface tension increases substantially. This increases the thin-film capillary number and thus results in film thinning (increase in β_f) at large λ (figure 17*b*).

3.4.3. *Comparison between variable-equilibrium and fixed-eqiibrium behaviour*

The behaviour described in § 3.4.1 and § 3.4.2 is strikingly different. For example, as λ increases in the variable-equilibrium case (equivalent to decreasing C_o), the system approaches the equilibrium response for a system where Marangoni stresses are non-existent. In contrast, near-equilibrium behaviour occurs as λ is decreased in the fixed-equilibrium studies. This difference in behaviour occurs due to the variation of $\mathrm{d}\gamma/\mathrm{d}\Gamma$ that exists in the variable-equilibrium studies and the variation in sorption rates necessary to maintain $\tilde{\Gamma}_{eq}$ in the fixed-equilibrium case.

The decrease in Γ with increasing λ in the variable-equilibrium-point system (figure 16*b*) is primarily due to the concurrent decrease in $\tilde{\Gamma}_{eq}$. In contrast, the decrease in Γ in the fixed-equilibrium-point system (figure 18*b*), where $\tilde{\Gamma}_{eq}$ is constant, is due to a decrease in C_s along the entire interface (figure 18*d*) as λ increases. Note that the thin-film value of C_s decreases with increasing λ in both the variable- and

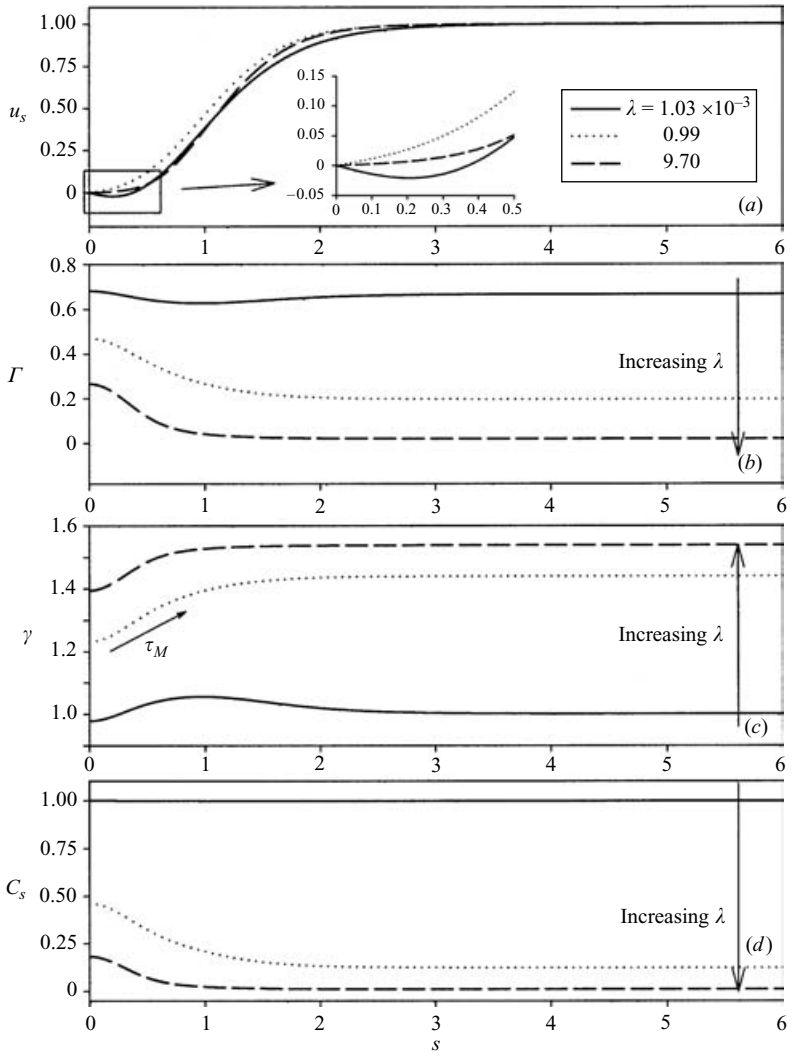

FIGURE 18. The influence of λ at a fixed $\tilde{\Gamma}_{eq}$ on the dimensionless (*a*) surface velocity, (*b*) surface concentration, (*c*) surface tension, and (*d*) sub-surface concentration along the interface for $\lambda = 1.03 \times 10^{-3}, 0.99, 9.70$. $St_a = \lambda St_d/(1 - \tilde{\Gamma}_{eq})$, $Ca = 0.15$, $El = 0.5$, $St_d = 5$, $Pe = 10$, $Pe_s = 10^3$.

fixed-equilibrium-point systems (figures 16*d* and 18*d*), as predicted by mass balance analysis. However, since $\tilde{\Gamma}_{eq}$ is held fixed in the fixed-equilibrium cases, far more surfactant is adsorbed to the interface, and thus the bulk concentrations are much lower than in the variable-equilibrium investigations (compare figure 16*d* and figure 18*d*).

The depletion of surfactant from the bulk is clearly evident in figure 19, which shows the bulk concentration field surrounding the semi-infinite bubble for $\lambda = 1.03 \times 10^{-3}$, 0.1, 9.07 at a fixed $\tilde{\Gamma}_{eq}$. At very low λ, the bulk concentration is nearly uniform and equal to the far-downstream value ($C = 1$). Under these conditions the system can be considered to be in bulk equilibrium. However, for large λ the surfactant in the thin film, Γ_{film}, is approximately non-existent because adsorption of surfactant is sufficient

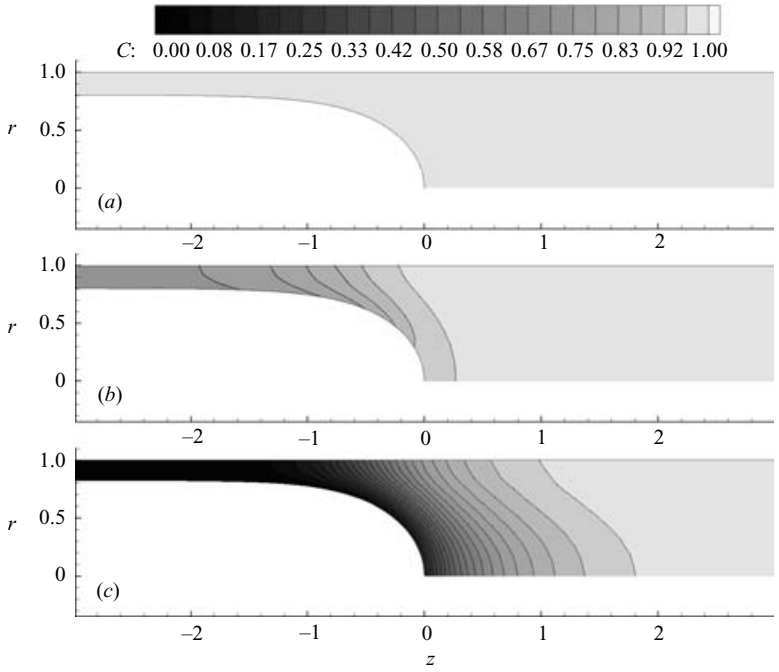

FIGURE 19. Bulk concentration field surrounding the semi-infinite bubble for (*a*) $\lambda = 1.03 \times 10^{-3}$, (*b*) 0.1, (*c*) 9.07 and constant $\tilde{\Gamma}_{eq}$ by concurrently varying $St_a = \lambda St_d/(1 - \tilde{\Gamma}_{eq})(Ca = 0.15, El = 0.5, St_d = 5, Pe = 10, Pe_s = 10^3)$.

to deplete the bulk of surfactant near the interface (figure 19*c*). As a result, very large concentration gradients develop in the bulk fluid. Under these conditions, C_s can be significantly less than the far-downstream value. Therefore at large λ, the transport of surfactant to the interface is limited by bulk transport processes.

4. Discussion

This study has examined the relationships between the physicochemical behaviour of surfactant and the behaviour of a steadily migrating semi-infinite bubble in a capillary tube. The behaviour of the system depends upon the macroscopic balances given in § 2.5 in concert with the surface tension of the transition region with respect to the thin film.

The analysis of § 2.5 shows that as the bulk concentration increases, λ decreases and $\tilde{C}_{film}$ increases. Thus larger bulk concentrations lead to reduced bulk concentration depletion in the thin film. Any depletion of surfactant from the thin film causes a rise in the surface tension to values greater than the equilibrium tension, γ_{eq}. The direction of the Marangoni stress depends on the surface tension in the transition region that exists between the tip and thin film – if the surface tension in the transition region is smaller than in the film, the film thickness increases and vice versa. However, the surface tension in the transition region is determined by surface convection and sorption kinetics.

Recall that in the absence of surfactant at small Ca a stagnation ring sweeps surfactant towards the tip and thin film (figure 6*b*). If surfactant kinetic exchange is slow (small St_a and St_d) or diffusive transport is slow (large Pe), the surface convection

drives surfactant out of the transition region into the thin film more rapidly than it can be replenished by sorption or diffusion. Consequently, the surface tension is higher in the transition region than in the film (see figure 11*c*), and the resulting Marangoni stress thins the film region. This behaviour is evident in figures 10(*b*) and 11(*c*) (at high *Pe*) and figures 13(*b*) and 14(*c*) (at low St_a).

In contrast, if kinetic or diffusive exchange is rapid (large St_a and St_d, small *Pe*), the transition region does not become depleted of surfactant, and the surface tension in the transition region is smaller than in the thin film (see figure 14*c* at large St_a). This drives flow to the thin film, and results in film thickening, as is demonstrated in figure 13(*b*) at large St_a. These observations are true at small *Ca*; however, at larger *Ca* the film is less depleted of surfactant because β_f increases. Consequently, the surface tension in the thin film decreases with increasing *Ca*, driving a Marangoni stress from the film to the transition region and modestly thinning the film (figures 4*b* and 5*c*).

Finally, the surfactant strength plays a role through the elasticity parameter, *El*. As *El* increases, the surface concentration is held more uniform because small concentration differences create large Marangoni stresses (see figure 8*b*, *c*) that in turn removes the recirculation region. The surface concentration is thus largely set by the depletion of bulk surfactant in the thin film, and hence at small *Ca* the surface concentration is uniformly low and the surface tension is large. The ensuing Marangoni stress from the tip to the thin film (figure 8*c*) causes a large film thickening effect that is shown in figure 7(*b*) at large *El*.

4.1. *Physiological significance*

The parameter variation studies presented above demonstrate that several surfactant physicochemical properties can influence the mechanics of bubble progression in rigid capillaries. Since this system mimics the continual interfacial expansion aspects of airway reopening, it is important interpret these results in terms of their potential physiological significance. In this section we discuss how changes in two system variables, β_f and Π_{tip}, could influence airway reopening mechanics.

The Rayleigh instability that may be responsible for the collapse or re-closure of opened airways is a function of the quantity of fluid coating the airway wall. Specifically, thicker films will result in an unstable system and therefore faster closure times will occur (Halpern & Grotberg 1993; Otis *et al.* 1993). As shown in figure 7(*b*), the thickness of the fluid coating the tube walls will decrease (increasing β_f) as the strength of the surfactant is increased. This decrease in fluid thickness would stabilize the lung by increasing the closure time. However, it should be noted that the percentage change in β_f ($\sim 4\%$) may not be sufficient to affect the stability of the system. Furthermore, the decrease in film thickness is accompanied by high surface tension (figure 8*c*), which may increase airway instability. Figure 13(*b*) indicates that β_f will increase as the sorption properties of the surfactant are reduced. In addition, figure 14(*c*) indicates that the magnitude of τ_M also increases as the sorption properties are reduced. Since a larger β_f as well as a larger τ_M can stabilize the lung (Halpern & Grotberg 1992; 1993; Otis *et al.* 1993), slow sorption properties may be beneficial from an airway closure standpoint. However, as demonstrated below, the elevation of Π_{tip} at low sorption rates can lead to a significant elevation in the stresses at the tube wall.

The epithelial cells that line the airway wall can be damaged by large compressive and shear (i.e. normal and tangential) stresses. Figure 20 shows the variation in the normal and tangential stress along the tube wall for $El = 10^{-3}$, 1.05, and 5.31. As *El*

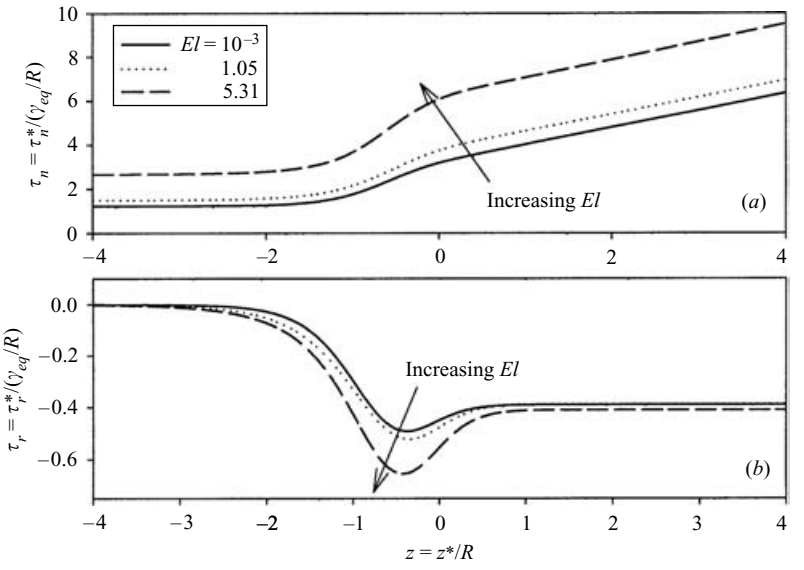

FIGURE 20. Variation of the dimensionless (*a*) normal and (*b*) shear stress along the tube wall for $El = 10^{-3}$, 1.05, 5.31 ($Ca = 0.15$, $St_a = 1$, $St_d = 5$, $\lambda = 0.1$, $Pe = 10$, $Pe_s = 10^3$).

increases, the pressure required to push the bubble forward, which is measured by Π_{tip}, also increases. As a result, the fluid pressures are elevated and large compressive stresses can develop (figure 20*a*) as Π_{tip} increases. In addition, the increase in Π_{tip} leads to an elevation of the wall shear stress near the bubble (figure 20*b*). Therefore, elevation of the reopening pressure can result in large normal and tangential stress at the airway wall. Since these stresses can damage the epithelial cells, which can lead to further surfactant inactivation, low Π_{tip} values are advisable to prevent lung injury. Since Π_{tip} decreases with increasing sorption rates (figure 13*a*), fast sorption properties would be beneficial from an airway reopening standpoint. However, as discussed above, these fast sorption properties may also lead to lung instability. Therefore, we hypothesize that an effective surfactant must have optimal sorption properties that balance low reopening pressures with the maintenance of stable airways.

5. Conclusions

The model described in this manuscript has been used to conduct an extensive parametric study that demonstrates the relationships between fluid flow and surfactant transport during the motion of a semi-infinite bubble in a capillary tube. The Marangoni parameter ($Ma = El/Ca$) was investigated by varying both the capillary (Ca) and elasticity (El) numbers independently while the influence of bulk diffusion was investigated by varying the bulk Péclet number (Pe). The effect of surfactant sorption properties was isolated by varying St_a and St_d simultaneously to maintain a fixed equilibrium point. Finally, the adsorption depth, λ, was investigated under variable- and fixed-equilibrium-point conditions.

The pressure drop across the interface at the bubble tip, Π_{tip}, contains a surface tension and viscous component. The surface tension component, $\gamma_{tip}\kappa_{tip}$, is elevated if the transport of surfactant to the interface is limited by either adsorptive or bulk transport processes. Under these conditions, the surface tension in the bubble

cap region, and thus γ_{tip}, can be significantly larger than the equilibrium value. For constant Ca, the viscous component, $4\,Ca\,\mathrm{d}u_s/\mathrm{d}s|_{tip}$, is governed by the tip surface velocity gradient. The generation of surface tension gradients can lead to the generation of Marangoni stresses, τ_M, near the bubble tip. These are responsible for removing the recirculating flow pattern from the interface and thus elevating $\mathrm{d}u_s/\mathrm{d}s|_{tip}$. In addition, τ_M can modify the surface tension component since the tip curvature, κ_{tip}, is governed by the local Marangoni stress field.

Large Π_{tip} values are physiologically significant since they can be correlated with an increase in the normal and shear stress at the tube wall. In addition, the quantity of fluid left behind in the thin film, measured by the dimensionless finger width, β_f, can be related to lung stability, which will be governed by the magnitude of τ_M as well as the thin-film surface tension, γ_{film}. When τ_M is directed towards the thin film, film thickening results (decrease in β_f) while when τ_M in the transition region is directed away from the thin film, film thinning results (increase in β_f). As the average γ increases to values greater than γ_{eq} due to low concentrations (large λ), capillary forces increase and result in a thinner film.

In summary, the current parameter variation study has demonstrated that the physicochemical properties can have a large impact on the mechanics associated with semi-infinite bubble progression in rigid capillaries. In future studies will use these computational techniques to simulate experimental conditions. Specifically, several dimensionless parameters will be varied concurrently to simulate the variation of the dimensional variables that can be controlled experimentally (i.e. U, C_o and surfactant type). More advanced computational approaches may include the formation of surfactant multilayers, which have been both observed (Takamoto *et al.* 2001) and modelled (Krueger & Gaver 2000), and simulation of remobilization kinetics where adsorption is rapid and the bulk concentration is large. Correlation of this computational model with experimental data will lead to a more complete description of the physicochemical properties of current pulmonary replacement surfactants. Identification of these properties and their effects on pulmonary mechanics may lead to more effect treatment strategies of diseases such as infant and acute respiratory distress syndrome.

We wish to thank the contribution of an anonymous reviewer to the Discussion section. This research was founded by the National Science Foundation grants (BES-9978605, DMS-9709754), the National Institutes of Health (R29-HL51334), and the NASA Physical Sciences Research Division (NAG3-2734).

REFERENCES

Bretherton, F. P. 1961 The motion of long bubbles in tubes. *J. Fluid Mech.* **10**, 166–188.

Eggleton, C. D., Pawar, Y. P. & Stebe, K. J. 1999 Insoluble surfactants on a drop in an extensional flow: a generalization of the stagnated surface limit to deforming interfaces. *J. Fluid Mech.* **385**, 79–99.

Enhörning, G. & Holm, B. A. 1993 Disruption of pulmonary surfactant's ability to maintain openness of a narrow tube. *J. Appl. Physiol.* **74**, 2922–2927.

Fairbrother, F. & Stubbs, A. E. 1935 Part VI The bubble-tube methods of measurement. *J. Chem. Soc.* **1**, 527–529.

Gaver, D. P. III, Halpern, D., Jensen, O. E. & Grotberg, J. B. 1996 The steady motion of a semi-infinite bubble through a flexible-walled channel. *J. Fluid Mech.* **319**, 25–65.

Gaver, D. P. III, Samsel, R. W. & Solway, J. 1990 Effects of surface tension and viscosity on airway reopening. *J. Appl. Physiol.* **69**, 74–85.

Ghadiali, S., Halpern, D. & Gaver, D. P. 2001 A dual-reciprocity boundary element method for evaluating bulk convective transport of surfactant in free-surface flows. *J. Comput. Phys.* **171**, 534–559.

Ghadiali, S. N. & Gaver, D. P. III 2000 An investigation of pulmonary surfactant physicochemical behavior under airway reopening conditions. *J. Appl. Physiol.* **88**, 493–506.

Ginley, G. M. & Radke, G. M. 1988 Influence of soluble surfactants on the flow of long bubbles through a cylindrical capillary. *ACS Symp. Series* **396**, 480–501.

Halpern, D. & Grotberg, J. B. 1992 Fluid-elastic instabilities of liquid-lined flexible tubes. *J. Fluid Mech.* **244**, 615–632.

Halpern, D. & Grotberg, J. B. 1993 Surfactant effects on fluid-elastic instabilities of liquid-lined flexible tubes: A model of airway closure. *Trans. ASME: J. Biomech. Engng* **115**, 271–277.

Johnson, R. A. & Borhan, A. 1999 Effect of insoluble surfactants on the pressure-driven motion of a drop in a tube in the limit of high surface coverage. *J. Colloid Interface Sci.* **218**, 184–200.

Kamm, R. D. & Schroter, R. C. 1989 Is airway closure caused by liquid film instability? *Respir. Physiol.* **75**, 141–156.

Krueger, M. A. & Gaver, D. P. III 2000 A theoretical model of pulmonary surfactant multilayer collapse under oscillating area conditions. *J. Colloid Interface Sci.* **229**, 353–364.

Levitzky, M. G. 1991 *Pulmonary Physiology*. McGraw-Hill.

Lipp, M. M., Lee, K. Y. C., Zasadzinski, J. A. & Waring, A. J. 1996 Phase and morphology changes in lipid monolayers induced by SP-B protein and its amino-terminal peptide. *Science* **273**, 1196–1199.

Lu, W. Q. & Chang, H. C. 1989 An extension of the biharmonic boundary integral method to free surface flows in channels. *J. Comput. Phys.* **77**, 340–360.

Macklem, P. T., Proctor, D. F. & Hogg, J. C. 1970 The stability of peripheral airways. *Respir. Physiol.* **8**, 191–201.

Martinez, M. J. 1987 *Viscous Flow of Drops and Bubbles in Straight and Constricted Tubes.* University of California, Berkeley.

Martinez, M. J. & Udell, K. S. 1989 Boundary integral analysis of the creeping flow of long bubbles in capillaries. *Trans. ASME* E: *J. Appl. Mech.* **56**, 211–217.

Milliken, W. J., Stone, H. A. & Leal, L. G. 1993 The effect of surfactant on the transient motion of Newtonian drops. *Physi. Fluids* A **5**, 69–79.

Myers, D. 1991 *Surfaces, Interfaces, and Colloids.* New York: VCH.

Otis, D. R. Jr., Johnson, M. Pedley, T. J. & Kamm, R. D. 1993 Role of pulmonary surfactant in airway closure: a computational study. *J. Appl. Physiol.* **75**, 1323–1333.

Perun, M. L. & Gaver, D. P. III 1995 Interaction between airway lining fluid forces and parenchymal tethering during pulmonary airway reopening. *J. Appl. Physiol.* **79**, 1717–1728.

Ratulowski, J. & Chang, H. C. 1990 Marangoni effects of trace impurities on the motion of long gas bubbles in capillaries. *J. Fluid Mech.* **210**, 303–328.

Reinelt, D. A. & Saffman, P. G. 1985 The penetration of a finger into a viscous fluid in a channel and tube. *SIAM J. Sci. Stat. Comput.* **6**, 542–561.

Shen, E. I. & Udell, K. S. 1985 A finite element study of low Reynolds number two-phase flow in cylindrical tubes. *Trans. ASME* E: *J. Appl. Mech.* **52**, 253–256.

Stebe, K. J. & Barthès-Biesel, D. 1995 Marangoni effects of adsorption-desorption controlled surfactants on the leading end of an infinitely long bubble in a capillary. *J. Fluid Mech.* **286**, 25–48.

Stone, H. A. 1990 A simple derivation of the time-dependent convective-diffusion equation for surfactant transport along a deforming interface. *Phys. Fluids* A **2**, 111–112.

Stone, H. A. & Leal, L. G. 1990 The effects of surfactants on drop deformation and breakup. *J. Fluid Mech.* **220**, 161–186.

Takamoto, D. Y., Lipp, M. M., von Nahmen, A., Lee, K. Y., Waring, A. J. & Zasadzinski, J. A. 2001 Interaction of lung surfactant proteins with anionic phospholipids. *Biophys J.* **81**, 153–169.

Taneva, S. G. & Keough, K. M. W. 1994 Dynamic surface properties of pulmonary surfactant proteins SP-B and SP-C and their mixtures with dipalmitoylphosphatidylcholine. *Biochemistry* **33**, 14660–14670.

Taylor, G. I. 1961 Deposition of a viscous fluid on the wall of a tube. *J. Fluid Mech.* **10**, 161–165.

Tchoreloff, P. A., Gulik, A., Denizot, B., Proust, J. E. & Puisieux, F. 1991 A structural study of interfacial phospholipid and lung surfactant layers by transmission electron microscopy after Blodgett sampling: influence of surface pressure and temperature. *Chem. Phys. Lipids* **59**, 151–165.

Westborg, H. & Hassager, O. 1989 Creeping motion of long bubbles and drops in capillary tubes. *J. Colloid Interface Sci.* **133**, 135–147.

Yap, D. Y. K. & Gaver, D. P. III 1998 The influence of surfactant on two-phase flow in a flexible-walled channel under bulk equilibrium conditions. *Phys. Fluids* **10**, 1846–1863.